Ref.TH.3713-CERN

A QCD MODEL FOR JET FRAGMENTATION INCLUDING SOFT GLUON INTERFERENCE

B.R. Webber *)
CERN - Geneva

A B S T R A C T

A new model for hadronic jet fragmentation in hard processes is presented. It is based on a QCD parton branching mechanism with correct treatment of leading collinear and infra-red singularities (i.e., including soft gluon interference). Hadronization occurs via preconfinement of colour singlet clusters, which decay according to a simple phase-space scheme. Although tightly constrained, the model gives a good account of existing e^+e^- annihilation data. It predicts significant differences between quark and gluon jets. Comparisons with data on the CERN $\bar{p}p$ collider jets suggest that a large fraction of them are gluon jets. The model predicts soft gluon interference effects in hadron distributions which are probably not yet observable for pions but should be clear for kaons and baryons.

*) On leave from the Cavendish Laboratory, University of Cambridge and Emmanuel College, Cambridge, U.K.

Ref.TH.3713-CERN
September 1983

1. - INTRODUCTION

The production of jets of hadrons is one of the most striking features of hard processes such as high-energy e^+e^- annihilation, deep inelastic lepton scattering and large-transverse-energy hadron collisions[1]. This phenomenon is widely regarded as evidence that short-distance interactions involve effectively pointlike hadronic constituents - partons. In quantum chromodynamics these partons are identified as quarks and gluons and their interactions are precisely specified[*]. The task of QCD is then to account not only for the features of jet production, such as cross-sections and jet axis angular distributions, but also for their fragmentation properties, such as angular sizes and hadronic multiplicities. This paper is concerned with the second of these objectives: the development of an understanding of jet fragmentation based on QCD.

Since around 1977, an appealing QCD description of jets has existed at the level of perturbation theory[3)-6)]. The presence of collinear singularities in gauge theories implies that a parton produced far off mass shell in a hard process will evolve by successive branching into a jetlike cascade of partons nearer to mass shell. Unfortunately, what happens next is not so clear, since it necessarily involves the long-distance, non-perturbative properties of the theory. Somehow these properties lead to the confinement of the partons in colourless bound states which we observe as hadrons, a process commonly called hadronization.

Eventually, non-perturbative techniques may provide sufficient understanding of confinement to permit the calculation of hadron distributions in jets from first principles. At present we are very far from such an understanding and it is necessary to resort to phenomenological models for the hadronization phase of jet development. For this reason the explanation of jet fragmentation cannot be said to be a definitive, fundamental test of QCD. Nevertheless, a satisfactory description based on the best possible treatment of perturbative jet development plus a plausible model for hadronization would constitute persuasive support for the theory.

The work reported here attempts to combine new developments on both fronts, viz. in QCD perturbation theory for parton jets and in the model for hadronization.

The new development in perturbative QCD is the calculation of leading infrared singularities as well as leading collinear singularities to all orders[7)-12)].

---

[*] See Refs. 2) for recent reviews of QCD.

Although quite recent, this work is already the subject of two extensive reviews[13),14)], to which the reader is referred for details. It is used here as the basis of a new Monte Carlo computer program for simulating parton jet evolution. The Monte Carlo approach has been shown by several authors[15)-22)] to be a convenient and powerful way of studying parton jets in the leading-collinear logarithmic approximation. The work on infra-red singularities shows, however, that this approximation seriously mistreats certain regions of phase space, most notably the region of soft gluon emission, which gives rise to the bulk of the parton multiplicity. Fortunately, the Monte Carlo procedure can be reformulated along the lines described in Ref. 23) to give a more correct treatment of soft gluon effects, even though they involve quantum interference phenomena, which one would not normally expect to be amenable to Monte Carlo techniques. In Section 2 of this paper the approach of Ref. 23) is reviewed briefly and extended from the purely gluonic case considered there to the full quark and gluon branching process.

Turning to the model for hadronization, a number of approaches have been tried with some success[24)-27)], notably the Feynman-Field model[24)] involving independent parton fragmentation and the Lund string model[26)]. The new development exploited here is the type of model[21),22),28)-30)] proposed by Wolfram[15)], which follows naturally from the "preconfinement" property already exhibited by jets at the perturbative level[31)]. Preconfinement is the tendency of the partons generated in the branching process to be arranged in colour-singlet clusters with limited extension in both co-ordinate and momentum space[6),32),33)]. It is natural to suppose that these clusters are the basic units out of which hadrons arise non-perturbatively. Their mass scale is controlled by the infra-red cut-off (minimum off-shellness) Q_0 at which perturbative branching is terminated. Wolfram's idea was to use a rather small value of Q_0 [and to enforce a non-perturbative splitting of gluons into quark-antiquark pairs[18)]], so that most clusters have masses of a few GeV or less and may be regarded as superpositions of resonances, with phase-space-dominated decay schemes into known resonances. Apart from its physical appeal, this approach has the attractive feature of introducing no free parameters or fragmentation functions to describe the transition from clusters to hadrons. Section 3 explains how such a model is combined with the new perturbative jet algorithm to give a complete Monte Carlo simulation of hadron distributions in jets.

In Section 4 the resulting predictions are compared in some detail with existing data on e^+e^- annihilation into hadrons*), a process in which the final states consist mainly of pairs of quark jets. Without introducing any additional parameters, the model also specifies the properties of gluon jets. The predicted characteristic differences between quark and gluon jets are discussed in Section 5, and in Section 6 comparisons are made with the properties of jets produced at the CERN $\bar{p}p$ collider, which are expected[34] to be mostly gluon jets.

An important difference between the work presented here and other approaches is the improved treatment of infra-red singularities, which leads to striking soft gluon interference effects at the parton level. The observability of these effects after hadronization is investigated in Section 7. Finally, Section 8 gives an overall summary of results and some conclusions.

2. - JETS IN PERTURBATIVE QCD

The basic picture of the perturbative phase of jet development in QCD is illustrated in Fig. 1. It is an iterative Markov branching process in which an initial parton far off mass-shell (with virtuality of the order of the scale Q^2 of the hard process in which it was produced) evolves into a cascade of partons nearer to mass-shell[5]. A parton branching vertex $i \to jk$ represents the splitting (with probability proportional to the running coupling constant α_s at an appropriate scale) of a parton of type i and virtuality q_i^2 into those of types j and k with virtualities $q_{j,k}^2$, normally much less than q_i^2. The distribution of the energy-momentum fraction in the splitting is given by the corresponding Altarelli-Parisi function $P_{i\to jk}(z)$ and the distribution of parton virtualities is controlled by a Sudakov-type form factor containing the appropriate virtual corrections.

The parton branching picture was originally based on the observation that leading collinear singularities are correctly given by the summation of dressed tree graphs in a physical gauge, neglecting interference. In that calculation, the whole phase space of kinematically allowed virtualities $q_{j,k}^2$ was available to the produced partons at each branching. The work of Refs. 7)-12) shows, however, that in the soft region, interference contributions, in which collinear logarithms may be replaced by infra-red ones, cannot be neglected. Their effect is to cancel completely (in leading logarithmic approximation) the branching probability for certain regions of phase space. The region that survives can be described in simple terms: it is the one in which successive opening angles in the branching process are ordered (uniformly decreasing).

*) Some preliminary comparisons were made in Ref. 28).

The angular ordering condition is normally applied to the variable

$$\xi \equiv q_j \cdot q_k / \omega_j \omega_k \qquad (1)$$

where $\omega_{j,k}$ are the energies of the produced partons. For negligible virtualities $q^2_{j,k}$ we have

$$\xi \simeq 1 - \cos\Theta \qquad (2)$$

where θ is the opening angle, and

$$q_i^2 \simeq 2\omega_j\omega_k\xi = 2z(1-z)\omega^2\xi \qquad (3)$$

where z is the energy fraction and ω is the energy of the parent parton i. Consequently the ordering of ξ is equivalent to that of q^2 when all parton energies are of the same order of magnitude but is a stronger constraint when soft partons are present. Since the Altarelli-Parisi functions have infra-red singularities for soft gluon emission, the principal effect of angular ordering is a strong suppression of the soft gluon component of the parton cascade. The suppression is a coherence phenomenon arising from the inability of long wavelength gluons to resolve the individual colour charges of partons within the jet. The jet, therefore, radiates soft gluons as a single source with the colour charge of the parton from which it originated*). The neglect of interference amounts to treating the jet as a set of incoherent sources and hence overestimates the soft gluon radiation.

The suppression of soft gluon emission due to coherence leads to a number of striking modifications in the properties of jets at the parton level[7)-14),23)]. Instead of peaking at low energies, corresponding to energy fractions x of order Q_0/Q, the parton energy distribution turns out to be suppressed up to values of order $\sqrt{QQ_0}$, giving a peak at $x \sim \sqrt{Q_0/Q}$. The distribution near the peak is roughly Gaussian in $\ln x$, with width proportional to $(\ln Q/\Lambda)^{3/4}$. Correspondingly, the parton rapidity distribution in e^+e^- final states has a dip instead of a plateau in the central region and the parton multiplicity is reduced relative to the no-interference prediction. The reduction is by a factor of $1/\sqrt{2}$ in the exponent of the asymptotic behaviour. In Sections 4-7 we shall see the extent to which these features at the parton level are reflected in hadron distributions, after hadronization according to the model described in Section 3.

---

*) An analogous effect in electrodynamics suppresses ionization and radiation from high energy e^+e^- pairs. See Ref. 35).

The QCD branching process with angular ordering to include soft gluon interference forms the basis of the Monte Carlo computer program used to calculate the predictions in this paper. It operates like the purely gluonic program described in Ref. 23) but includes quarks (five flavours) and the hadronization model to be discussed in the next section. Starting from a specified parton source with energy E and initial angular variable $\xi_0 \leq 1$ ($\theta_0 \leq \pi/2$), it develops a parton cascade until further branching would be inconsistent with the assumed set of quark masses m_q and gluon mass cut-off Q_0. The threshold in ξ for the branching $i \to jk$ is

$$\xi_{min} = (Q_j + Q_k)^2/\omega^2 \tag{4}$$

where Q_j represents the relevant quark mass m_q if j is a quark and Q_0 if it is a gluon. Above this threshold the probability distribution of ξ for the branching is given by a Sudakov-type form factor:

$$\frac{d\mathcal{P}_{i\to jk}}{d\xi} = \frac{d}{d\xi}\,\frac{\Delta_{i\to jk}(\xi_{max})}{\Delta_{i\to jk}(\xi)} \tag{5}$$

where

$$\ln \Delta_{i\to jk}(\xi_{max}) = -\int_{\xi_{min}}^{\xi_{max}} \frac{d\xi}{\xi} \int_{z_{min}}^{z_{max}} dz\, \frac{\alpha_s}{2\pi}\, P_{i\to jk}(z) \quad . \tag{6}$$

Because ξ is ordered, the upper limit ξ_{max} is simply the ξ value of the previous branching. By a straightforward generalization of the argument in Ref. 23), the limits on the energy fraction may be well approximated by

$$\begin{aligned} z_{min} &= Q_j/\omega\sqrt{\xi} \\ z_{max} &= 1 - Q_k/\omega\sqrt{\xi} \end{aligned} \quad . \tag{7}$$

For the argument of α_s I use $2z^2(1-z)^2\omega^2\xi \simeq q_T^2$, the relative transverse momentum squared:

$$\alpha_s = \frac{1}{b \ln\left[2z^2(1-z)^2\omega^2\xi/\Lambda^2\right]} \tag{8}$$

where $b = (11N_c - 2N_f)/12\pi$ for N_c colours and N_f flavours. This incorporates certain infra-red logarithms in the limits $z \to 0, 1$ [32),36)]. It means, however, that the form factors (6) cannot be evaluated in closed form. For the important processes $q \to qg$ and $g \to gg$, they are computed in the Monte Carlo program by interpolation in tables prepared in advance. The relatively uncommon process $g \to q\bar{q}$ has no soft singularities so such complications would be unwarranted. In this case, I replace $z^2(1-z)^2$ by a constant in Eq. (8) and also make the approximation of neglecting z_{min} and $1 - z_{max}$ in Eq. (6), to obtain

$$\Delta_{g\to q\bar{q}}(\xi) \simeq \left[\frac{\ln(\omega^2\xi/\tilde{\Lambda}^2)}{\ln(4m_q^2/\tilde{\Lambda}^2)}\right]^{-1/6\pi b} \tag{9}$$

where $\tilde{\Lambda}$ is some constant times Λ. The probability distribution (5) may then be generated simply by choosing

$$\xi = \frac{\tilde{\Lambda}^2}{\omega^2}\left(\frac{\omega^2\xi_{max}}{\tilde{\Lambda}^2}\right)^{R^{6\pi b}} \tag{10}$$

where R is a random number between zero and one. For gluon branching a ξ value must be chosen according to (10) for every open $g \to q\bar{q}$ channel and by interpolation for $g \to gg$; the actual branching selected is the one with the largest ξ value.

After all branching has terminated, the masses of the produced partons are set at the corresponding cut-off values Q_j and their momenta are computed from their energies ω_j, the angular variables ξ, and a random azimuthal orientation for each branching. All the momenta generated are guaranteed to lie within phase space because the dynamical constraint of ξ ordering is stronger than pure kinematics. In this respect the angular ordering procedure is simpler and more efficient than earlier Monte Carlo algorithms ignoring interference, which had to take explicit account of kinematic phase space constraints.

The new procedure has a number of peculiar features, some of which are discussed in more detail in Ref. 23). Being formulated in terms of angles and energies, it is not manifestly covariant. For a given value of the total energy E, jet properties depend on the arbitrary initial opening angle θ_0. The invariant mass and state of motion of the jet source cannot be specified in advance but must be deduced from the energies and angular variables in the cascade after

branching has terminated. This last peculiarity is actually the key to understanding how Lorentz invariance is satisfied. After computing the invariant mass Q of the source, one may transform the whole cascade to its rest frame. Then, one finds that for a given value of Q the jet properties are, to a good approximation, independent of the initial conditions on E and θ_0. The choice of a very small value of θ_0, for example, will lead to the generation of jets with rapidly-moving sources and $Q \ll E$. In the original frame they look very narrow, but in their rest frames they look just like jets of the same invariant mass generated at larger θ_0.

The lack of manifest covariance means that it is incorrect to simulate multijet production by combining single cascades generated in different frames. Furthermore, as explained in Ref. 23), difficulties in the choice of gauge and the definition of the energy fraction z are avoided, and the kinematics simplified, by requiring all branching to take place in a single hemisphere ($\xi \leq 1$). Therefore, in e^+e^- annihilation, for example, the entire final state must be generated as a "photon jet", starting from the initial vertex $\gamma \to q\bar{q}$ with $\theta_0 \leq \pi/2$ and developing the quark and antiquark jets simultaneously in the same hemisphere. Afterwards, we may compute the Q^2 of the virtual photon and transform to its rest frame, where the jets will become back-to-back and event properties at a given Q^2 will be independent of θ_0. If instead we tried to generate separate quark and antiquark jets with $E = \frac{1}{2} Q$ and to combine them back-to-back directly, the results would always be θ_0-dependent because parton emission into the region $\theta_0 < \theta < \pi - \theta_0$ would be arbitrarily forbidden.

3. - HADRONIZATION

The mechanism adopted here for hadron formation in jets is close to that proposed by Wolfram[15] and used in a number of recent jet studies ignoring interference[21),22),29),30)], so the discussion in this section will concentrate on points of difference from these other similar schemes.

As mentioned in the Introduction, the central idea is the formation, at the end of the perturbative phase of jet development, of colour singlet clusters of partons, which subsequently decay to hadrons. The dominant colour index structure (the leading term in the $1/N_c$ expansion) for a diagram such as Fig. 1 can be represented, after re-ordering of external lines if necessary, in a planar form as depicted in Fig. 2. Then adjacent index pairs can form colour singlet clusters, represented by the blobs, provided the two indices associated with each gluon are dynamically separated. It is assumed that this occurs through a non-perturbative low q^2 enhancement of the splitting $g \to q\bar{q}$, which is relatively uncommon in the perturbative branching process.

The approximation scheme (9) and (10) for the $g \to q\bar{q}$ form factor has the advantage of permitting such an enhancement to be built in automatically. If we make the choice of parameters

$$\tilde{\Lambda} = 2m_0 = Q_0 \tag{11}$$

in Eq. (10), where m_0 is the light (u,d) quark mass, then ξ will always be above threshold for $g \to q_0\bar{q}_0$ and all gluons will eventually decay into quark-antiquark pairs*). Like the "gluon mass" Q_0, m_0 is a cut-off related to the confinement scale - more analogous to a constituent quark mass than a current quark mass - so Eq. (11) is not unreasonable. A rescaling of $\tilde{\Lambda}$ is formally a higher order correction, so the leading behaviour of the perturbative branching is unchanged. What happens in practice is that the amount of $g \to q\bar{q}$ branching generated agrees with perturbative expectations until ξ is close to the light quark threshold, at which point the gluons suddenly decay.

The resulting mass distribution of colour singlet clusters (blobs in Fig. 2) is illustrated in Fig. 3. Note the characteristic features of preconfinement: the distribution peaks at low mass, falls off steeply at high mass, and is Q^2 independent. It presumably represents a smeared version of the spectrum of "primordial resonances" formed in the early stages of confinement in real jets. It seems reasonable, therefore, to treat the fragmentation of the clusters as a kind of averaged resonance decay with much of the dynamics washed out, leading to:

i) quasi-two-body decay, which usually predominates for known resonances;

ii) branching ratios determined by density of states, i.e., phase space times spin degeneracy;

iii) no spin correlations, and hence isotropic decay.

The Monte Carlo procedure adopted for cluster decay is accordingly as follows. For a cluster formed from quark-antiquark flavours $q_1\bar{q}_2$, another flavour q_3 or d_3 is chosen at random, where q_3 = u, d, or s and d_3 is one of the six corresponding diquarks. The flavours of the decay products are then taken to be $(q_1\bar{q}_3)$ and $(q_3\bar{q}_2)$ (two-meson decay) or $(q_1 d_3)$ and $(\bar{q}_2\bar{d}_3)$ (baryon-antibaryon decay). Each decay product is selected from a list of resonances with the appropriate flavour, weighted according to the spin degeneracy $(2S+1)$, and the available phase space is tested against a random number. If the test is failed, another flavour q_3 or d_3 is chosen and the

*) The gluon form factor (9) is not defined for $\tilde{\Lambda} = 2m_q$ because gluons cannot appear as outgoing external lines, but the branching probability distribution (5) is still well defined.

procedure is repeated. The list of resonances used consists of the 0^-, $1^\pm$ and 2^+ SU(3) nonets of mesons and the $\frac{1}{2}^+$ octet and $\frac{3}{2}^+$ decuplet of baryons. To work well the scheme should presumably saturate the resonance spectrum up to the cluster mass scale for all flavours and baryon numbers. To avoid bias, however, it seemed preferable not to include incomplete SU(3) multiplets, which tend to lack strange members.

Notice that in the above procedure the produced quark-antiquark $q_3\bar{q}_3$ (or diquark-antidiquark $d_3\bar{d}_3$) functions only as a flavour label and has no dynamical attributes. The dynamical suppression of strange particle or baryon production in cluster decay comes entirely from the resonance spectrum via the reduction of phase space for these channels. Correspondingly, the "intrinsic transverse momentum" generated in hadronization is determined by the average energy release in cluster decay (and in the subsequent cascade decay of produced resonances). Such properties of the hadronization process are not described by additional parameters in this type of approach, but are supposed to arise from the observed spectrum and decay systematics of resonances. It is assumed that this information is sufficient to incorporate all the relevant non-perturbative features of QCD.

For very massive clusters the assumption of isotropic decay becomes unreasonable, so the program allows for the option of anisotropic fission before decay above some fission threshold, M_f. At most a small fraction of clusters are involved (typically, about 1 in 10 has mass $M_C > 4$ GeV - see Fig. 3) so the fission algorithm is not crucial. The following simple "symmetrical string breaking" scheme was adopted. For a cluster of mass $M_C > M_f$ formed from a (di)quark of momentum p_1^μ and an anti(di)quark of momentum p_2^μ, the fission $C \to X + Y$ is assumed to yield,

$$p_X^\mu = \left(1 - \frac{Q_0}{M_C}\right) p_1^\mu + \frac{Q_0}{M_C} p_2^\mu \quad , \tag{12}$$

$$p_Y^\mu = \left(1 - \frac{Q_0}{M_C}\right) p_2^\mu + \frac{Q_0}{M_C} p_1^\mu \quad ,$$

so that

$$M_X^2 \sim M_Y^2 \sim Q_0 M_C \tag{13}$$

while

$$(p_X - p_1)^2 \sim (p_Y - p_2)^2 \sim Q_0^2 \quad . \tag{14}$$

This roughly corresponds to the process depicted in Fig. 4: a string with energy density Q_0 per unit rapidity breaks in the middle through production of a quark-antiquark pair with virtuality of order Q_0^2. The flavour of the produced pair is taken to be $u\bar{u}$, $d\bar{d}$ or $s\bar{s}$ with equal probability. If necessary the process is repeated for the fission fragments X and Y, until all clusters are below the fission threshold M_f, whereupon ordinary isotropic decay commences as outlined above.

For clusters containing heavy (c or b) quarks the decay model must be modified, complete data on heavy flavour resonance multiplets not being available. The heavy quark is assumed to undergo free-particle β decay, giving two hadronic clusters (as illustrated in Fig. 5 for a charmed cluster) or one cluster plus leptons. In the case of $b \to c$ decay, the process is repeated on the produced charmed cluster. This model is clearly too crude to predict details of heavy flavour decay distributions, but it gives roughly correct associated multiplicities and should be adequate for the broad features of event structure with which we shall be concerned.

4. - COMPARISON WITH DATA ON $e^+e^- \to$ HADRONS

The model described in Sections 2 and 3 has three parameters: the QCD scale Λ, the gluon mass cut-off Q_0, which fixes the scale at which hadronization sets in, and the fission threshold M_f, above which anisotropic cluster splitting occurs. In addition, there are the (constituent) quark mass parameters, but as explained in Section 3 the light quark masses were fixed by Eq. (11),

$$m_u = m_d = \tfrac{1}{2} Q_0 \quad , \tag{15}$$

and the heavier quarks were given their customary masses:

$$m_s = 0.5\ \text{GeV}, \quad m_c = 1.5\ \text{GeV}, \quad m_b = 5.0\ \text{GeV}. \tag{16}$$

The Table summarizes the dependence on Λ, Q_0 and M_f of some important observables in e^+e^- annihilation at c.m. energy $Q = 34$ GeV, where there are especially good experimental data. The parameter dependence is generally small. In the case of Λ and Q_0, this is due to compensation between the perturbative and non-perturbative phases of jet development. A combination of these parameters leading to a high mass scale for colour singlet clusters implies less perturbative branching but more hadron production per cluster, and vice versa. The compensation starts to break down when (as in the first column of the Table) the cluster mass scale becomes so large that the resonance multiplets available

to the hadronization model substantially fail to saturate the spectrum up to that scale. The dependence on the fission threshold is weak because, as explained in Section 3, anisotropic fission is a refinement affecting only a small fraction of clusters.

For comparisons with experimental data from now on, the parameter values

$$\Lambda = 0.25 \text{ GeV}, \quad Q_0 = 0.6 \text{ GeV}, \quad M_f = 4 \text{ GeV} \qquad (17)$$

will be used. These seem physically reasonable values [for example Eq. (15) then implies light constituent quark masses of 300 MeV] and they give satisfactory agreement with the data in the Table, except for the $K^{\pm}$ multiplicity, which will be discussed below.

Figure 6a shows an event generated by the Monte Carlo program at $Q = 34$ GeV. The event starts with $u\bar{u}$ pair production and seven colour singlet clusters are formed after QCD branching. The clusters range in mass from 0.8 to 3.2 GeV/c and decay into 2-5 hadrons each. It happens that two baryon-antibaryon pairs and two $K^{\pm}$ pairs are produced in this event, together with 11 charged and 5 neutral pions.

Figure 6b shows the hadron momenta in the event plane (i.e., the plane that minimizes Σp^2_{out}), with the sphericity axis in the horizontal direction. We see that the event has a three-jet structure, the third jet arising from the hard bremsstrahlung gluon emitted early in the cascade by the u quark. This accounts for the rather high hadron multiplicity (18 charged hadrons vs. an average of 12). The numbering scheme in the figure shows the strong extent to which the fast hadrons follow the directions of their parent partons, with relatively soft hadrons between the jets taking care of colour neutralization.

Figures 7[37)-41)] and 8[42)] show the single particle inclusive cross-sections for various types of produced hadrons as functions of the c.m. energy fraction, $x = 2E_i/Q$. Note that the theoretical predictions are absolutely normalized and that both theory and experiment are weighted by $s/\beta = Q^2c/v$, where v is the hadron velocity, to minimize the kinematic scaling violation at low x. The agreement between the predictions and experiment, in both shape and normalization, is generally very good. The largest discrepancy occurs in the normalization of the $K^{\pm}$ distribution (Fig. 7c), for which the prediction is too low. The same discrepancy is of course also seen in the $K^{\pm}$ average multiplicity (Fig. 9[38)] and the Table). On the other hand, the predicted neutral kaon production agrees well with experiment (Fig. 8). The problem is that the TASSO[38),42)] results show a 40% excess of charged over neutral kaon production, whereas the

model predicts a much smaller excess of about 5%, coming from the enhancement of $\gamma \to u\bar{u}$ over $d\bar{d}$ at the primary vertex. The large isospin asymmetry in the data needs further investigation; if confirmed, it will cause problems for any model and might be due to some unexpected feature of heavy flavour production or decay.

The predicted overall charged multiplicity is shown in Fig. 10[39),43)-46)]. Bearing in mind that the systematic errors in the data [$\sim\pm1.5$ for JADE[45)] and $\sim\pm0.9$ for TASSO[46)]] are not shown in the figure, the agreement with experiment is satisfactory, although the prediction may be slightly low. Above $b\bar{b}$ threshold, it follows remarkably closely the expected asymptotic behaviour[6)-9),47)]:

$$\langle n(Q)\rangle \propto \left(\ln\frac{Q}{\Lambda}\right)^{p} \exp\left(c\ln\frac{Q}{\Lambda}\right)^{1/2} \qquad (18)$$

where (for five flavours)

$$p = -\frac{1}{4} - \frac{N_f}{6\pi b}\left(1-\frac{C_F}{C_A}\right) = -0.492 \quad , \qquad (19)$$

$$c = 4C_A/\pi b = 6.26$$

$$\left[C_F = (N_c^2-1)/2N_c = 4/3 \ , \ C_A = N_c = 3\right] \quad , \qquad (20)$$

the constant of proportionality in Eq. (18) being 0.103 when Λ = 0.25 GeV. The power p in Eq. (19) is, strictly speaking, a non-leading effect which can be reliably computed only by including higher-order QCD corrections. Surprisingly, however, it appears that the approach of Section 2, applied to leading-order terms only, gives the same result for p as a full treatment including higher-order terms[12)]. The effects of higher-order terms will be discussed further in Section 6. The exponent c in Eqs. (18) and (20) is not affected by them.

The predicted multiplicity distribution agrees well with experiment [Fig. 11[48)]], reproducing the observed approximate KNO scaling[49)] behaviour throughout the presently-accessible energy range. This is, however, a transient phenomenon unrelated to the exact KNO scaling predicted by QCD at astronomically high energies[5),6),9)]. For example, the ratio of mean to dispersion, $\langle n\rangle/D$, is observed, and predicted, to be about three in this energy range, whereas the asymptotic prediction is

$$\left(\langle n\rangle/D\right)_{e^+e^-} \xrightarrow[Q^2\to\infty]{} \sqrt{6C_F/C_A} = 1.63 \quad . \qquad (21)$$

The discrepancy is due to large non-leading corrections which decrease extremely slowly with Q^2 (like $\sqrt{\alpha_s}$ rather than α_s), as discussed in Ref. 23).

Figures 12[50),51)]-16[52)] show various predictions relating to transverse momenta and event shape, all of which agree well with experiment.

The rapidity distribution of charged hadrons is shown in Fig. 17. The predicted distribution has a slight dip at zero rapidity, which is a reflection of that in the parton distribution due to soft gluon interference. It is interesting that the visibility of the dip is predicted to depend strongly on the correct choice of rapidity axis. As shown in Fig. 18, the dip is present if the thrust axis is used but practically disappears if one changes to the sphericity axis, which is less sensitive to the event structure in the soft region. In Fig. 17, for both the prediction and the data, the thrust axis was used and the rapidities were computed assuming all particles to have the pion mass. The overall agreement between theory and experiment is quite good, but at $Q = 29$ GeV the prediction falls some 10-20% below the data for $y < 2$. The significance of this discrepancy is not yet completely clear, because systematic errors (not shown) are important in this region and more recent preliminary data suggest a smaller value[53)]. As for the dip at zero rapidity, there is some indication of a turnover in the $Q = 29$ GeV data below $y \simeq 1$, but a more thorough study must await precise information at $y < 0.4$, together with some experimental investigation of the effects of rapidity axis errors as discussed above.

Finally, Fig. 19[54)] summarizes the Q^2 dependence of charged particle production in various intervals of the c.m. momentum fraction, x_p. Corresponding to the deficiency at low rapidities in Fig. 17, the absolute normalization of the prediction is slightly too low at the smallest x_p values; it is also a little too high at large x_p. The slopes of the curves agree well with the trend of the data in each x_p interval, showing that the amount of scaling violation predicted is about right.

As an overall conclusion, we may say that the model accounts quite well and naturally for the broad features of the existing e^+e^- annihilation data. This is particularly encouraging in view of the small number of parameters in the model, and the rather weak dependence of the predictions on them, as exhibited in the Table. There is a problem with the large observed charged/neutral kaon ratio which, if confirmed, might demand a more sophisticated treatment of heavy flavours. There are also indications, in the average multiplicity and in the rapidity and x_p distributions, of a 10-20% deficiency in the predicted amount of soft hadron production. This could be because the suppression of soft gluon emission, arising from completely destructive interference in the leading logarithmic approximation, is less strong when non-leading corrections are included. This point will be discussed in a little more detail in Section 7.

It is interesting to compare the results presented above with those obtained by Field and Wolfram[21] using a similar hadronization model but neglecting interference effects in the QCD branching process. They found that an enhancement of gluon bremsstrahlung (a large value of Λ) was necessary to account for the rate of increase of $\langle p_T^2 \rangle$ (Fig. 12), but that this gave rise to excessive scaling violation in the x_p distribution, especially at low x_p. Gottschalk[22] showed that this conflict can be resolved if one uses a small value of Λ but makes instead an ad hoc enhancement of bremsstrahlung early in the QCD cascade, where most of the transverse momentum is generated. Such an effect emerges naturally here from the more correct treatment of infra-red singularities. First, the argument of α_s becomes q_T^2 rather than q^2, giving more bremsstrahlung for a given value of Λ. Second, the angular ordering constraint due to interference is more restrictive later in the cascade, when the allowed angular region for branching becomes very small. Therefore, the enhancement of gluon emission survives only in the earlier part of the cascade, leading to $\langle p_T^2 \rangle$ values and scaling violations of the correct magnitudes.

The results obtained here for the mean charged multiplicity (Fig. 10) are surprisingly close to those of Field and Wolfram. As already remarked, they also exhibit the expected asymptotic behaviour (18), in which the exponent c has the value (20), which is only one half that given by neglecting interference. It follows that the treatment of Field and Wolfram must generate non-leading terms which mimic such a change in c over the currently-accessible range of Q^2. At $Q = 100$ GeV, the results obtained by Gottschalk[22], in a version of their model including many refinements but still neglecting interference, are beginning to show a more rapid rate of increase of multiplicity, due to the incorrect value of the exponent.

5. - EXPECTED PROPERTIES OF GLUON JETS

The e^+e^- final states examined in the previous section are all pairs of quark jets, in the sense that they all develop from an initial quark-antiquark pair. It is interesting to consider how their properties would differ if the initial pair of partons were gluons rather than quarks, leading to a pair of gluon jets*). An attractive feature of the hadronization scheme described in Section 3 is that it does not involve independent fragmentation functions for quarks and gluons, so the properties of gluon jets are already prescribed by the set of parameters (17) used in the study of e^+e^- data.

---

*) See also Refs. 55) for discussion of the expected properties of gluon jets.

Accordingly, a Monte Carlo sample of pairs of gluon jets was generated, starting each QCD cascade with a colour-singlet, scalar ($F_{\mu\nu}F^{\mu\nu}$) source. It was checked for quark jets that the quantities of interest are not sensitive to whether the source is a Lorentz vector (as in e^+e^- annihilation) or scalar, but this could not be done for gluons because there is no corresponding simple colour-singlet vector source.

The most striking differences between the quark and gluon jet events occurred in their multiplicity, rapidity, thrust and sphericity distributions, as summarized by the dot-dashed curves in Figs. 10, 11 and 15-17.

The average multiplicity for gluon jets is predicted to be substantially higher than that for quark jets, as indicated in Fig. 10. This is due to the greater colour charge of the gluon, which leads to increased gluon bremsstrahlung. The resulting asymptotic prediction,

$$\langle n \rangle_{gg} / \langle n \rangle_{q\bar{q}} \xrightarrow{Q^2 \to \infty} C_A / C_F = 9/4 \quad , \tag{22}$$

is well known[5),6),9)]. However, the approach followed here implies a smaller ratio (about 1.6) in the energy range of Fig. 10, owing to large subasymptotic corrections. As in the case of corrections to the KNO scaling prediction (21), these are of order $\sqrt{\alpha_s}$, i.e., proportional to $\ell n^{-1/2}(Q/\Lambda)$. Figure 20 shows that the Monte Carlo results are entirely consistent with the expected behaviour, the convergence to the asymptotic result (22) being extremely slow. Unfortunately, the subasymptotic terms are sensitive to higher-order QCD corrections which have not yet been computed, so the prediction in Fig. 20 is not reliable. The moral is that, while we may expect the average multiplicities of gluon jets to be substantially bigger than those of quark jets, the quantitative prediction (22) is probably so asymptotic as to be useless and we urgently need a full calculation of the $O(\sqrt{\alpha_s})$ correction to this result.

In proportion to the average multiplicity, the multiplicity distribution for gluon jets is expected to be considerably narrower than that for quark jets (Fig. 11). The asymptotic prediction[5),6),9)],

$$\left(\frac{\langle n \rangle}{D}\right)_{q\bar{q}} \Big/ \left(\frac{\langle n \rangle}{D}\right)_{gg} \xrightarrow{Q^2 \to \infty} \sqrt{\frac{C_F}{C_A}} = \frac{2}{3} \quad , \tag{23}$$

agrees fairly well with the Monte Carlo results in this case, owing to a cancellation of large subasymptotic corrections.

Figures 15-17 show that the predicted extra multiplicity in gluon jets is connected with their larger angular size: compared with quark jets, they have higher mean sphericity and lower mean thrust, and their rapidity distributions are more concentrated at lower rapidities (larger angles relative to the thrust axis). Indeed, we see from Fig. 17 that the expected hadron production at high rapidities is actually reduced for gluon jets, so that the mean multiplicity inside a given cone around the thrust axis would be less (for a sufficiently small cone, e.g., for a half-angle less than 15° at $Q = 29$ GeV) for a gluon jet than for a quark jet. This illustrates the importance of taking into account the experimental cuts used to define jets before trying to test predictions about their properties.

It is important also to remember that the definition of all e^+e^- hadronic final states as pairs of quark jets necessarily includes those with manifest three-jet or multijet configurations (e.g., Fig. 6), which form the high-sphericity, low-thrust tail of the event distribution. The "pairs of gluon jets" generated for the study in this section contain an even greater fraction of multijet configurations, owing to the higher probability of gluon bremsstrahlung from gluons. The proportion of clear multijet events is, however, strongly dependent on the definition of a jet. It is also not very reliably predicted by a leading-logarithmic approach. Consequently, it does not seem worthwhile to try to separate out this class of events in the present analysis.

6. - COMPARISON WITH $\bar{p}p$ COLLIDER DATA

The jets observed[56)-59)] in CERN $\bar{p}p$ collider events at high transverse energies are expected, from QCD calculations of production cross-sections[34)], to be mostly gluon jets. It is therefore of great interest to see whether they exhibit any of the above characteristic differences from the jets observed in e^+e^- annihilation. To investigate this, Monte Carlo jet-jet pairs were generated with the observed angular and dijet mass distributions, and then subjected as far as possible to the same selection procedures as the experimental data.

A difficulty in the experimental study of the collider jets is their contamination by additional particles not associated with the jets, coming instead from initial-state gluon bremsstrahlung or spectator parton fragmentation. This background was of course absent from the pairs of jets generated for the Monte Carlo study, so the experimental selection cuts applied to remove it had to be assumed to be fully efficient in doing so. On the other hand, the same cuts inevitably also remove some genuine jet fragments. It was possible to study the effects of this on the observed properties of the Monte Carlo jets. In general, the effects were quite large, precluding any direct comparison with e^+e^- data not subjected to the same selection procedures.

The data of the UA2 collaboration[58] on the charged particle multiplicity in collider jets are shown in Fig. 21[43),46),58),60),61)], together with the model predictions for quark and gluon jets. The difference between Figs. 21a and b illustrates the importance of the procedure adopted to eliminate the background of unassociated particles. In Fig. 21a an upper limit on the background was estimated from the charged particle distribution in $\Delta\phi$, the azimuthal angle (around the beam axis), taking the axis of the jet of largest transverse energy to define $\Delta\phi = 0$.

The background subtraction consisted of removing a uniform distribution in $\Delta\phi$, with a particle density equal to that observed around $\Delta\phi = \pi/2$. This procedure also removes a large fraction of the true jet multiplicity, $\Delta\phi = \pi/2$ corresponding loosely to the central rapidity region in the dijet centre-of-mass frame. Furthermore, it is clear from Fig. 17 that the fraction removed from gluon jets will be larger than that from quark jets. Thus the model predictions after subtraction are closer together, as shown in Fig. 21a, which also shows e^+e^- data modified by the same procedure. In Fig. 21b an estimated correction for this effect has been applied to the data, which may then be compared with unsubtracted predictions and e^+e^- results. The conclusion in either case is that the observed multiplicity lies above that predicted for quark jets and close to that for gluon jets, in qualitative agreement with the expected predominance of gluon jet production.

The UA2 data on the azimuthal flow of transverse energy are compared with the predictions for quark and gluon jets in Fig. 22. The theory and data are absolutely normalized, but a small ($\lesssim 4$ GeV) constant background has been added to the theoretical values so that they coincide with the data around $\Delta\phi = \pi/2$. The background of unassociated particles is much less of a problem here than in the case of the multiplicity, because although numerous they carry little transverse energy. We see that the general features of the data are well reproduced by the model, with the angular widths of the jets tending to be somewhat greater than those expected for quark jets and in better agreement with the predictions for gluon jets[*)]. The greater apparent width of the opposite-side ($\Delta\phi \simeq \pi$) jet is due to acollinearity of the jet axes arising from the net transverse momentum of the dijet system, the observed distribution of which was incorporated in the Monte Carlo jet axis distribution.

---

*) A small sample of Monte Carlo jets were processed through a full simulation of the UA2 detector to check that this qualitative conclusion was not affected by the finite resolution of the detector.

Data from the UA1 collaboration[59] on jet fragmentation into charged particles are shown in Figs. 23 and 24. Here, particles are not associated with a jet unless they lie inside a cone of half-angle 35° centred on the jet axis. This criterion hardens the observed distribution of the longitudinal momentum fraction z (Fig. 23), which again lies between the model predictions for quark and gluon jets (except at $z > 0.7$, where the observed cross-section is somewhat larger than both predictions, but still extremely small). The integrals under the curves show that the predicted average charged multiplicities, after cuts, are 5.8 for quark jets and 8.1 for gluon jets (averaged over $E_T > 30$ GeV), which are similar to the results expected after the UA2 background subtraction procedure, as depicted in Fig. 21a.

The observed transverse momentum (p_T) distribution (Fig. 24) is influenced by the 35° cone criterion, by a cut on $z > 0.1$, and by the definition of p_T (relative to the vector sum of charged particle momenta within the cone). After these cuts, the predictions for quark and gluon jets are practically indistinguishable over a wide range of p_T. At low p_T the gluon jet distribution is somewhat less peaked. The overall normalization for gluon jets is now well below that for quark jets, owing to their softer z distribution (Fig. 23) and the cut on z. Once again, the data are in surprisingly good agreement with expectations for a mixture of quark and gluon jets.

The conclusion from the above comparisons with collider jet data is that the model predictions, using the same parameter values as for e^+e^- annihilation at lower energies, certainly look qualitatively reasonable and suggest that a majority of the jets produced have the fragmentation properties expected for gluon jets. Further analysis, based on the much larger data sample obtained in 1983 collider running, should allow more detailed comparisons and more quantitative estimates of the fraction of gluon jets, which could then be compared with the gluon fractions predicted independently by QCD calculations of production cross-sections.

7. - LOOKING FOR SOFT GLUON INTERFERENCE

The expected effects of soft gluon interference in the perturbative phase of jet development were summarized in Section 2. The hadronization model described in Section 3 leads to corresponding features in the predicted hadron distributions. Some of these have been mentioned in Section 4, viz., charged multiplicities in agreement with Eq. (18), reduced hadron production at low rapidities (Figs. 17 and 18) and reduced scaling violation for a given rate of increase of $\langle p_T^2 \rangle$.

The most striking interference effect at the parton level is undoubtedly the approximately Gaussian peak at $x \sim \sqrt{Q_0/Q}$ in the parton (or cluster) $\ell n\, x$ distribution. As shown in Fig. 25, a corresponding peak should appear in hadron distributions. The principal effect of hadronization, at least in the model used here, is simply to shift the peak to lower values of x. Roughly speaking, the unphysical parameter Q_0 is replaced by a physical scale, Q_h, of the order of the mass of the observed hadron, so that the peak is asymptotically at

$$x \sim \sqrt{Q_h/Q} \qquad \text{(high } Q^2\text{)} \qquad (24)$$

Empirically, it seems that the model gives

$$Q_h \simeq m_h/2 \quad . \qquad (25)$$

At low Q^2, phase space limitations take over, giving a peak position which varies more like

$$x \sim Q_c/Q \qquad \text{(low } Q^2\text{)} \qquad (26)$$

where Q_c is set by the typical hadronic cluster mass: $Q_c \simeq 1.5$ GeV, from Fig. 3.

Since most of the charged particles in jets are pions, Eq. (25) implies that the peak in the charged $\ell n\, x$ distribution occurs at very low x, corresponding to a momentum of the order of 1 GeV/c even at the highest attainable energies (Fig. 26). Furthermore, the transition from the "kinematic" behaviour (26) to that characteristic of interference, Eq. (24), will occur at

$$Q_{trans} \sim Q_c^2/Q_h \sim 4.5/m_h \text{ GeV} \qquad (27)$$

which is around 30 GeV for pions. Therefore, we cannot expect to confirm Eq. (24) for charged particles at currently accessible e^+e^- energies, although it should be possible at the next generation of e^+e^- machines. In $\bar{p}p$ collider events, the peak is probably obscured by the large background of unassociated low-momentum hadrons.

The situation is better if particle identification is available, for then the $\ell n\, x$ distributions of heavier particles can be studied*). According to Eq. (27), the characteristic interference behaviour (24) should set in for kaons

*) The importance of looking at heavy particle spectra for interference effects, essentially for the reasons given here, was emphasized in Ref. 9).

and baryons at energies well within the range of existing e^+e^- machines. This is because the momentum distributions of heavy hadrons more accurately reflect that of the colour singlet clusters discussed in Section 3, which shows a strong interference peak. For pions, there is more momentum smearing due to cluster decay and the true interference peak does not become visible until higher Q^2.

The only problem with heavy particle spectra is that very high statistics are required to locate the peak. It may be useful to note that, according to the model predictions, the peak should be fairly symmetrical in the variable $\ell n\, x_p$, where x_p is the momentum fraction (see Fig. 25). Consequently, the mean value of $\ell n\, x_p$, which might be easier to measure, follows the peak rather closely. The Monte Carlo results on this quantity are summarized in Fig. 27. We see that for kaons and protons, but not for pions, it has the characteristic interference behaviour (24) for energies above 10 GeV.

As in other tests of QCD, non-leading corrections could lead to substantial changes in quantitative predictions, such as those in Figs. 26 and 27. The situation here is worse than usual, because the corrections are of order $\sqrt{\alpha_s}$ rather than α_s. Figure 20 should remind us that there is no conceivable energy at which such corrections are strictly negligible. At present, they are known in only a few cases[12]. For the average parton multiplicity, the subleading factor which behaves like a power of $\ell n\, Q/\Lambda$ is unchanged: as already remarked in Section 4, the power is still given by Eq. (19). This is true for both quark and gluon jets. On the other hand, the peak in the parton $\ell n\, x$ distribution is raised and shifted to lower x. This suggests that the strength of the destructive interference in the soft region is reduced by non-leading corrections. In the absence of any systematic procedure for including such corrections in the QCD branching process, we cannot estimate the resulting changes in hadron distributions. It appears likely, however, that they will be in the direction of increasing soft hadron production and shifting the $\ell n\, x$ peak to even lower x values.

8. - CONCLUSIONS

The aim of the work summarized in this paper was to combine recent improvements in the treatment of the soft component of QCD jets with the physically appealing hadronization scheme of Wolfram. The resulting model is not exactly simple but it probably has the least complexity (and the fewest parameters) consistent with incorporating current QCD-based ideas about jet fragmentation.

On the whole, the model, with the rather natural choice of parameters given in Eq. (17), does remarkably well in accounting for the main features of a wide range of experimental data. In e^+e^- annihilation, the spectra of identified hadrons, transverse momentum distributions, event shapes and the multiplicity

distribution are all well described. The improved treatment of soft gluons seems to eliminate earlier difficulties[21] in reconciling the amount of scaling violation with the rate of increase of transverse momenta. It may lead to slightly too much suppression of soft hadron production, but non-leading QCD corrections are likely to counteract this effect.

Comparisons of the model with recent data on jet fragmentation in $\bar{p}p$ collider events are also encouraging. In interpreting these data, one has to take account of the selection cuts applied to exclude particles not associated with the jets, which inevitably modify observed jet properties. The Monte Carlo approach on which the model is based is well suited to dealing with this problem. Taking the cuts into account, the data suggest that the fragmentation of collider jets is somewhat different from that expected for quark jets. According to the model, there are characteristic differences between quark and gluon jets, arising mainly from the larger angular size of the latter. The multiplicities, energy flow patterns and momentum distributions of the collider jets all deviate from those expected for quark jets in the directions expected if a large proportion of them are gluon jets.

The soft gluon interference effects incorporated in the model, together with the hadronization scheme adopted, imply an interference peak in hadronic momentum fraction ($\ell n\, x_p$) distributions. For pions, the peak is shifted to low momenta and its position does not show the Q^2 dependence characteristic of interference until very high energies. For kaons and baryons the reduced momentum smearing in cluster decay should lead to an earlier onset of the characteristic Q^2 dependence. This prediction seems well worth experimental investigation.

In conclusion, one should remark on the several respects in which the present model might be improved. On a phenomenological level, a better treatment of heavy flavour hadronization[29] would permit the study of charmed particle distributions, for example, and might somehow account for the peculiar experimental data on charged/neutral kaon production in e^+e^- annihilation.

The model might also be extended to describe the QCD branching of incoming, space-like partons as well as that of outgoing, timelike ones. This would permit the Monte Carlo generation of entire $\bar{p}p$ collider events, as in Refs. 62) and 63), instead of isolated pairs of jets. For consistency, soft gluon interference effects should be included throughout the process. However, these effects are not yet fully understood in the case of spacelike branching, so further theoretical work is required before this could be attempted.

Most fundamentally, it would be good to be able to incorporate non-leading QCD corrections, both of the conventional $O(\alpha_s)$ type[64] (e.g., for the study of three-jet configurations in e^+e^- final states) and also those of $O(\sqrt{\alpha_s})$ which come from the infra-red region[12]. There are indications that the latter would lead to additional soft hadron production, which may be called for by the e^+e^- data in the central region at high Q^2. For some interesting quantities, such as the ratio of multiplicities in quark and gluon jets, the $O(\sqrt{\alpha_s})$ corrections could be extremely important but they have not yet been calculated. Again, therefore, more theoretical work will have to be completed before one knows precisely how the model should be modified.

ACKNOWLEDGEMENTS

It is a pleasure to acknowledge valuable theoretical discussions with M. Ciafaloni, T.D. Gottschalk, G. Ingelman, G. Marchesini and A.H. Mueller. I am also grateful to R.K. Bock, L. Fayard, P. Mättig and A. Weidberg for help and advice about experiments, although they should not be held responsible for my interpretation of the data.

Λ (GeV) Q_0 M_f	0.18 0.80 ∞	0.18 0.40 ∞	0.18 0.40 4	0.25 0.60 ∞	0.25 0.60 4	Experiment Refs. 37),38)
$\langle S \rangle$	0.16	0.12	0.10	0.13	0.11	0.13±0.04
$\langle T \rangle$	0.89	0.90	0.92	0.90	0.91	0.89±0.02
$\langle p_L \rangle$	1.83	1.57	1.62	1.64	1.54	1.48±0.11
$\langle p_T \rangle$	0.59	0.44	0.42	0.52	0.43	0.46±0.11
$\langle n_{\pi^\pm} \rangle$	7.0	8.6	9.4	8.5	9.6	10.3 ±0.4
$\langle n_{K^\pm} \rangle$	0.8	0.8	1.0	1.0	1.2	2.0 ±0.2
$\langle n_{p^\pm} \rangle$	1.2	0.5	0.4	0.8	0.6	0.8 ±0.1

TABLE - Dependence of various e^+e^- annihilation properties on model parameters at $Q = 34$ GeV.

REFERENCES

1) G. Wolf, in Proc. 21st Int. Conf. on High Energy Physics, Paris, 1982, Journal de Physique C3 (1982) 525.

2) W. Marciano and H. Pagels, Phys. Rep. 36 (1978) 138;
Yu.L. Dokshitzer, D.I. Dyakonov and S.I. Troyan, Phys. Rep. 58 (1980) 269;
E. Reya, Phys. Rep. 69 (1981) 195;
A.H. Mueller, Phys. Rep. 73 (1981) 237;
G. Altarelli, Phys. Rep. 81 (1982) 1.

3) G. Altarelli and G. Parisi, Nucl. Phys. B126 (1977) 298.

4) G. Sterman and S. Weinberg, Phys. Rev. Lett. 39 (1977) 1436.

5) K. Konishi, A. Ukawa and G. Veneziano, Nucl. Phys. B157 (1979) 45.

6) A. Bassetto, M. Ciafaloni and G. Marchesini, Nucl. Phys. B163 (1980) 477.

7) A.H. Mueller, Phys. Lett. 104B (1981) 161.

8) B.I. Ermolaev and V.S. Fadin, JETP Lett. 33 (1981) 269.

9) Yu.L. Dokshitzer, V.S. Fadin and V.A. Khoze, Phys. Lett. 115B (1982) 242; Z. Phys. C15 (1982) 325; Z. Phys. C18 (1983) 37;
V.S. Fadin, Yad. Fiz. 37 (1983) 408.

10) A. Bassetto, M. Ciafaloni, G. Marchesini and A.H. Mueller, Nucl. Phys. B207 (1982) 189.

11) M.G. Ryskin, Yad. Fiz. 36 (1982) 965.

12) A.H. Mueller, Nucl. Phys. B213 (1983) 85; Columbia Univ. preprint CU-TP-263 (1983); private communication of errata (to be published).

13) A. Bassetto, M. Ciafaloni and G. Marchesini, Phys. Rep. (to be published).

14) L.V. Gribov, E.M. Levin and M.G. Ryskin, Phys. Rep. (to be published).

15) S. Wolfram, in Proc. 15th Rencontre de Moriond (1980), ed. J. Tran Thanh Van.

16) G.C. Fox and S. Wolfram, Nucl. Phys. B168 (1980) 285.

17) R. Odorico, Nucl. Phys. B172 (1980) 157; Phys. Lett. 102B (1981) 341;
P. Mazzanti and R. Odorico, Phys. Lett. 95B (1980) 133; Z. Phys. C7 (1980) 61.

18) K. Kajantie and E. Pietarinen, Phys. Lett. 93B (1980) 269.

19) F.E. Paige and S.D. Protopopescu, Brookhaven report BNL 31987 (1982).

20) S. Ritter, Z. Phys. C16 (1982) 27.

21) R.D. Field and S. Wolfram, Nucl. Phys. B213 (1983) 65.

22) T.D. Gottschalk, Nucl. Phys. B214 (1983) 201.

23) G. Marchesini and B.R. Webber, CERN preprint TH.3525 (1983).

24) R.D. Field and R.P. Feynman, Nucl. Phys. B136 (1978) 1.

25) A. Ali, E. Pietarinen, G. Kramer and J. Willrodt, Phys. Lett. 93B (1980) 155.

26) B. Andersson, G. Gustafson and C. Peterson, Z. Phys. C1 (1979) 105;
B. Andersson, G. Gustafson and T. Sjöstrand, Z. Phys. C6 (1980) 235;
T. Sjöstrand, Computer Phys. Comm. 27 (1982) 243;
B. Andersson, G. Gustafson, G. Ingelman and T. Sjöstrand, Phys. Rep. (to be published).

27) S. Ritter and J. Ranft, Acta. Phys. Pol. B11 (1980) 259.

28) B.R. Webber, in Proc. 18th Rencontre de Moriond (1983), ed. J. Tran Thanh Van.

29) T.D. Gottschalk, Caltech preprint CALT-68-1006 (1983).

30) T.D. Gottschalk, Caltech preprints CALT-68-1030, 1052, 1059 (1983).

31) D. Amati and G. Veneziano, Phys. Lett. 83B (1979) 87.

32) D. Amati, A. Bassetto, M. Ciafaloni, G. Marchesini and G. Veneziano, Nucl. Phys. B173 (1980) 429.

33) G. Marchesini, L. Trentadue and G. Veneziano, Nucl. Phys. B181 (1981) 335.

34) R. Horgan and M. Jacob, Nucl. Phys. B179 (1981) 441.

35) A.E. Chudakov, Izv. Akad. Nauk. SSSR, ser. fiz. 19 (1955) 650.

36) Yu.L. Dokshitzer, JEPT Lett. 46 (1977) 641;
G. Parisi, Phys. Lett. 90B (1980) 295;
G. Curci and M. Greco, Phys. Lett. 92B (1980) 175;
M. Ciafaloni, Phys. Lett. 95B (1980) 113;
M. Ciafaloni and G. Curci, Phys. Lett. 102B (1981) 352.

37) CELLO Collaboration,
H.-J. Behrend et al., Z. Phys. C14 (1982) 189.

38) TASSO Collaboration,
M. Althoff et al., Z. Phys. C17 (1983) 5, and references therein.

39) DASP Collaboration,
R. Brandelik et al., Nucl. Phys. B148 (1979) 189.

40) D.L. Sharre et al., Phys. Rev. Lett. 41 (1978) 1005.

41) TASSO Collaboration,
R. Brandelik et al., Phys. Lett. 108B (1982) 71.

42) TASSO Collaboration,
R. Brandelik et al., Phys. Lett. 105B (1981) 75.

43) SLAC-LBL Collaboration,
G.G. Hanson, in Proc. 13th Rencontre de Moriond (1978), ed. J. Tran Thanh Van.

44) PLUTO Collaboration,
Ch. Berger et al., Phys. Lett. 78B (1978) 176; 81B (1979) 410.

45) JADE Collaboration,
W. Bartel et al., Phys. Lett. 88B (1979) 171.

46) TASSO Collaboration,
R. Brandelik et al., Phys. Lett. 89B (1980) 418.

47) W. Furmanski, R. Petronzio and S. Pokorski, Nucl. Phys. B155 (1979) 253;
K. Konishi, Rutherford Laboratory preprint RL-79-035 (1979).

48) PLUTO Collaboration,
Ch. Berger et al., Phys. Lett. 95B (1980) 313.

49) Z. Koba, H.B. Nielsen and P. Olesen, Nucl. Phys. B40 (1972) 317.

50) TASSO Collaboration,
R. Brandelik et al., Phys. Lett. 86B (1979) 243.

51) PLUTO Collaboration,
Ch. Berger et al., Phys. Lett. 86B (1979) 413, 418.

52) TASSO Collaboration,
R. Brandelik et al., Z. Phys. C4 (1980) 87.

53) P. Mättig, private communication.

54) TASSO Collaboration,
R. Brandelik et al., Phys. Lett. 114B (1982) 65.

55) B.R. Webber, Physica Scripta 25 (1982) 198;
L.M. Jones and R. Migneron, Z. Phys. C16 (1983) 217.

56) UA2 Collaboration,
M. Banner et al., Phys. Lett. 118B (1982) 203.

57) UA1 Collaboration,
G. Arnison et al., Phys. Lett. 123B (1983) 115.

58) UA2 Collaboration,
P. Bagnaia et al., CERN preprint EP/83-94 (1983).

59) UA1 Collaboration,
G. Arnison et al., CERN preprint EP/83-118, EP/83-119 (1983).

60) A.G. Clark et al., Nucl. Phys. B160 (1979) 397.

61) R. Plunkett, Ph.D. Thesis, Cornell University (1983).

62) G.C. Fox and R.L. Kelly, in Proton-Antiproton Physics (A.I.P. Conference Proc. No. 85, 1981);
R. D. Field, G.C. Fox and R.L. Kelly, Phys. Lett. 119B (1982) 439.

63) R. Odorico, Nucl. Phys. B199 (1982) 189; Bologna preprint IFUB 82/20 (1982); CERN preprint TH.3662 (1983).

64) J. Kalinowski, K. Konishi and T.R. Taylor, Nucl. Phys. B181 (1981) 221, 253.

FIGURE CAPTIONS

Fig. 1 : Perturbative QCD branching process following $e^+e^- \to q\bar{q}$.

Fig. 2 : Dominant colour index structure of Fig. 1. The blobs represent colour singlet clusters to be used as the basis for hadronization.

Fig. 3 : Distribution of colour singlet cluster mass, M_c, in e^+e^- annihilation at c.m. energies $Q = 35$ GeV and 53 GeV. Parameter values: $\Lambda = 0.25$ GeV, $Q_0 = 0.60$ GeV.

Fig. 4 : String model for fission of clusters with $M_c > M_f$.

Fig. 5 : Simplified model used for heavy flavour decay.

Fig. 6 : Monte Carlo event at c.m. energy $Q = 34$ GeV.
(a) Schematic time development;
(b) Final hadron c.m. momenta in event plane.

Fig. 7 : Single-particle inclusive cross-sections, $e^+e^- \to hX$. Data from Refs. 37)-41). In this and subsequent figures, "QCD MC" refers to the QCD Monte Carlo model prediction with parameter values given by Eq. (17).

Fig. 8 : Inclusive cross-sections for neutral strange particles. Data from Ref. 42).

Fig. 9 : Charged particle average multiplicities as functions of c.m. energy, Q. Data from Ref. 38).

Fig. 10 : Overall mean charged multiplicity in $e^+e^- \to$ hadrons. Data from Refs. 39), 43)-46). In this and subsequent figures the dot-dashed curves show the model predictions when quark jets are replaced by gluon jets (i.e., for gg production instead of $q\bar{q}$).

Fig. 11 : KNO-scaled charged multiplicity distribution. Data from Ref. 48).

Fig. 12 : Mean square transverse momentum, relative to the sphericity axis, as a function of c.m. energy. Data from Refs. 50) and 51).

Fig. 13 : Transverse momentum distribution, relative to the sphericity axis. Data from Ref. 50).

Fig. 14 : Distributions of mean square transverse momenta in and out of the event plane. Data from Ref. 50).

Fig. 15 : Average value of (1-thrust) versus c.m. energy. Data from Ref. 52).

Fig. 16 : Average sphericity versus c.m. energy. Data from Ref. 52).

Fig. 17 : Charged particle rapidity distribution, relative to the thrust axis. Data from Ref. 46).

Fig. 18 : Dependence of the predicted rapidity distribution on the choice of rapidity axis.

Fig. 19 : Dependence on c.m. energy-squared of the charged particle momentum fraction distribution ($x_p = 2\,|p_{cm}|/Q$). Data from Ref. 54).

Fig. 20 : Predicted ratio of average multiplicities in quark and gluon jets. The points show the Monte Carlo results and their statistical errors (4000 events per point). The line is a fit of the form $\langle n\rangle_g/\langle n\rangle_q = 9/4 - A(\ell n\, E/\Lambda)^{-1/2}$, which gives $A \approx 1.28$. To save computer time, for this figure single jets of energy E were generated and the multiplicity ratio was computed for clusters, without hadronization.

Fig. 21 : Mean charged particle multiplicities in jets. Data from Refs. 43), 46), 58), 60), 61).
(a) Data and predictions after cuts to eliminated unassociated particles [see text and Ref. 58)];
(b) Corrected UA2 data, compared with model predictions and lower-energy data.

Fig. 22 : Azimuthal distribution of transverse energy (E_T) in $\bar{p}p$ collider jets, where the azimuth $\Delta\phi$ is measured with respect to the axis of the jet of highest E_T. Data from Ref. 58) and model predictions are shown for three different ranges of E_T for that jet.

Fig. 23 : Distribution of the longitudinal momentum fraction, z, for charged particles in $\bar{p}p$ collider jets with $E_T > 30$ GeV. z is defined as the component of the momentum along the jet axis, divided by the energy of the jet. Data from Ref. 59).

Fig. 24 : Transverse momentum distribution for $z > 0.1$ charged particles in $\bar{p}p$ collider jets with $E_T > 30$ GeV. The selection cuts and definition of p_T are explained in the text. Data from Ref. 59).

Fig. 25 : Model predictions of the charged particle momentum fraction distribution in gluon jets, showing the interference peak. The momentum fraction is defined in the dijet centre-of-mass frame: $x_p = 2|p_{cm}|/Q$, where Q is the dijet invariant mass.

Fig. 26 : Predicted position of the peak in the charged particle momentum fraction distribution, as a function of dijet invariant mass, Q.
(a) Value of $\ell n\, 1/x_p$ at the peak. The dashed lines show the expected high and low Q^2 behaviours (24) and (26).
$[Q_h \simeq 0.075$ GeV, $Q_c \simeq 1.5$ GeV$]$.
(b) Corresponding value of the momentum (in the dijet c.m. frame) at the peak.

Fig. 27 : Predicted mean values of $\ell n\, 1/x_p$ for different types of charged hadrons in e^+e^- final states. The dashed lines show the expected asymptotic behaviour (24) $[Q_h \simeq 0.075$, 0.30 and 0.50 GeV for $\pi^\pm$, $K^\pm$ and $p/\bar{p}$, respectively$]$.

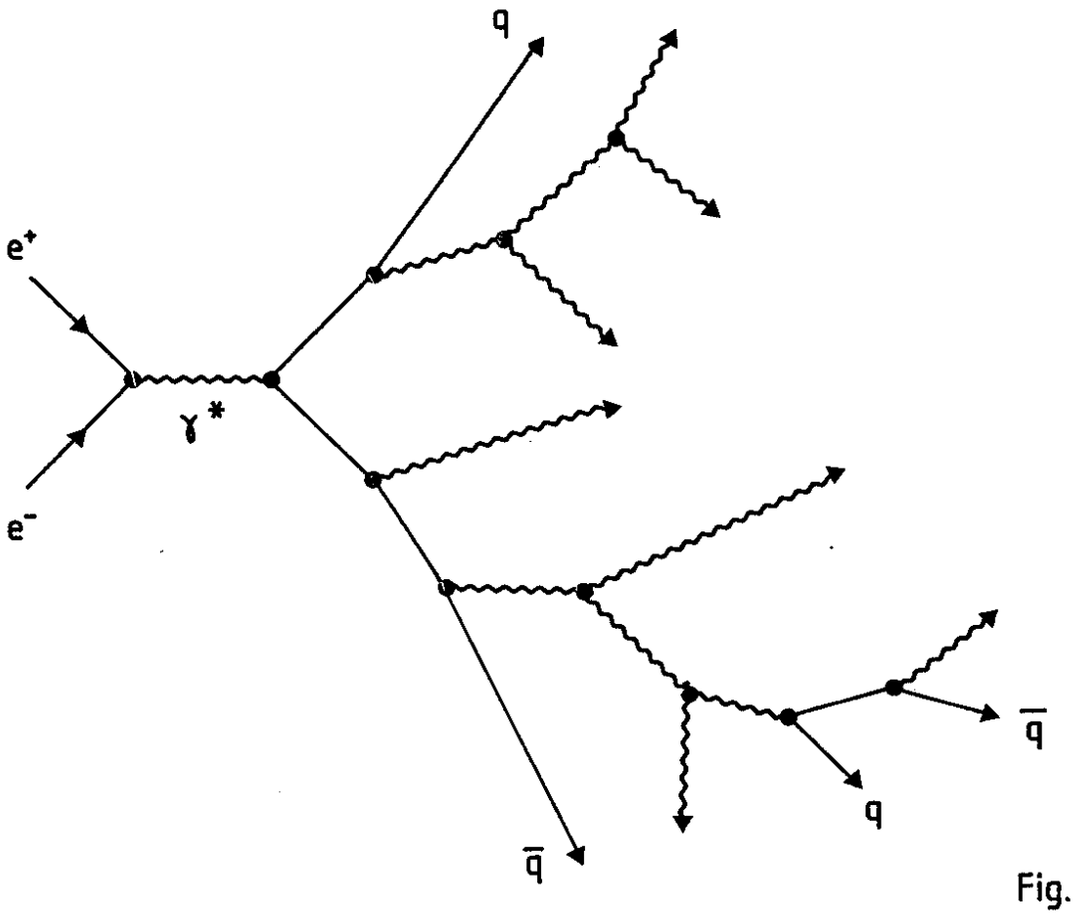

Fig. 1

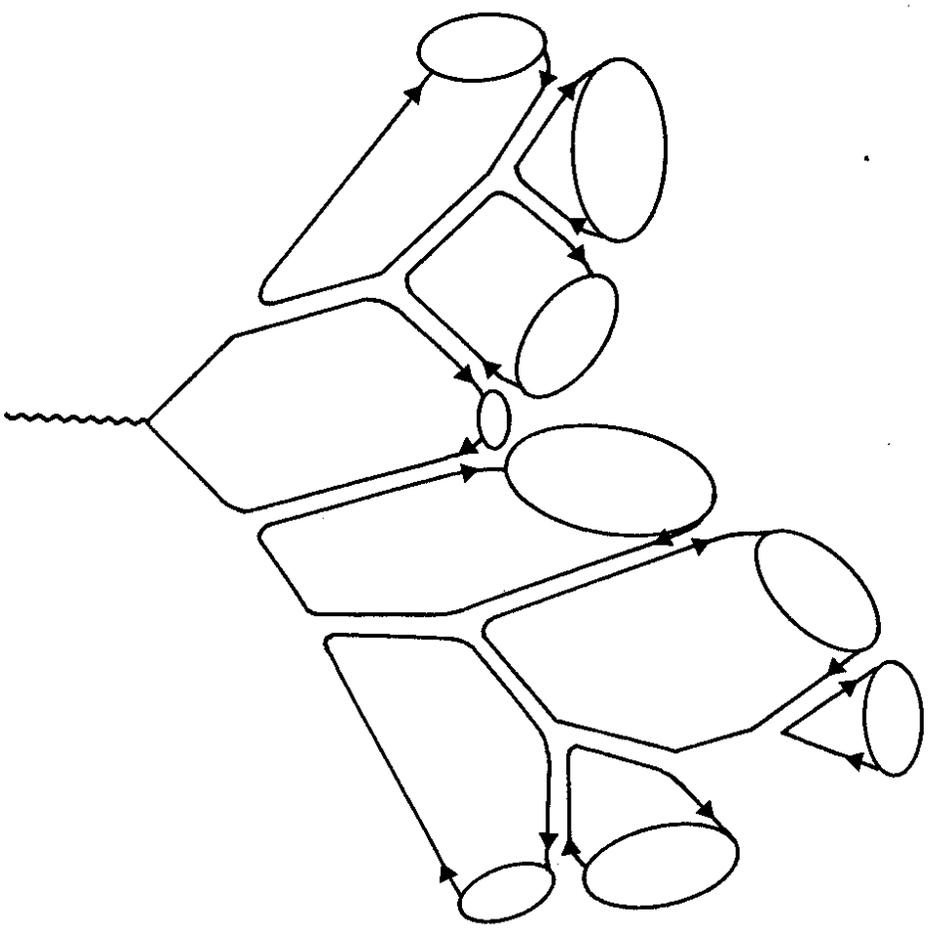

Fig. 2

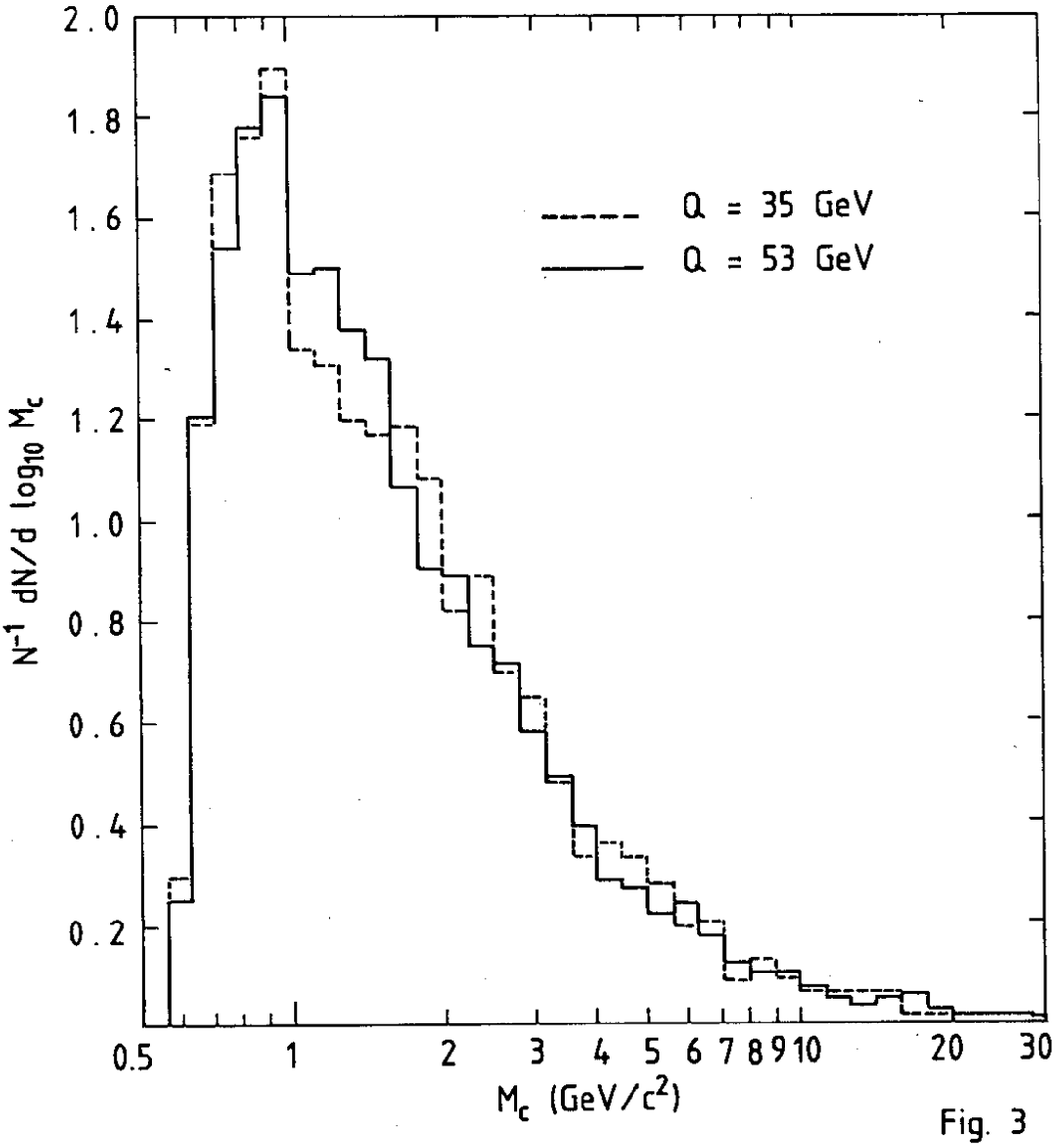
2.0
1.8
1.6
1.4
1.2
1.0
0.8
0.6
0.4
0.2
N^{-1} dN/d $\log_{10} M_c$
Q = 35 GeV
Q = 53 GeV
0.5
1
2
3
4
5
6
7
8
9
10
20
30
M_c (GeV/c^2)

Fig. 3

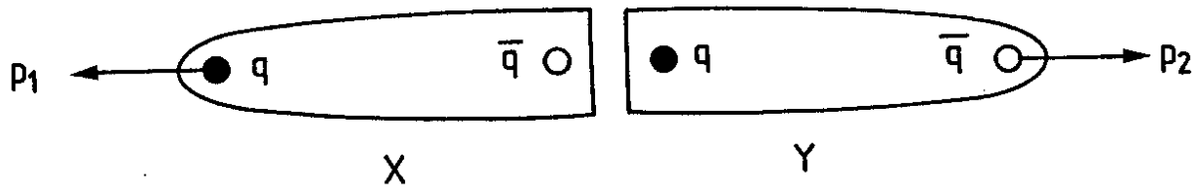

Fig. 4

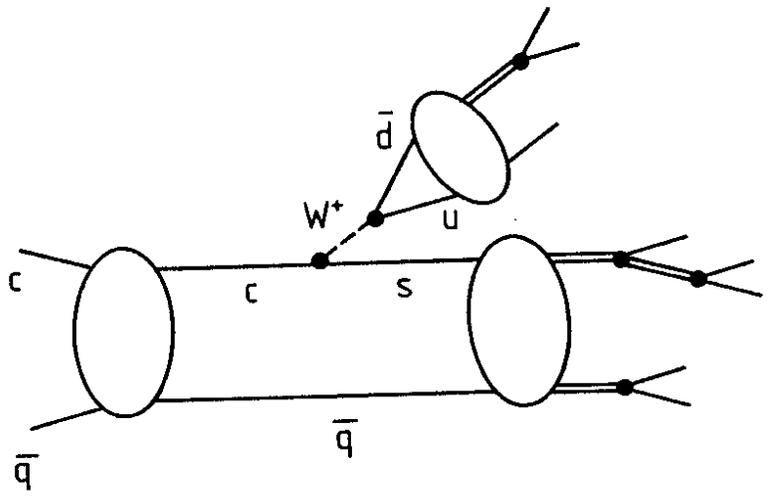

Fig. 5

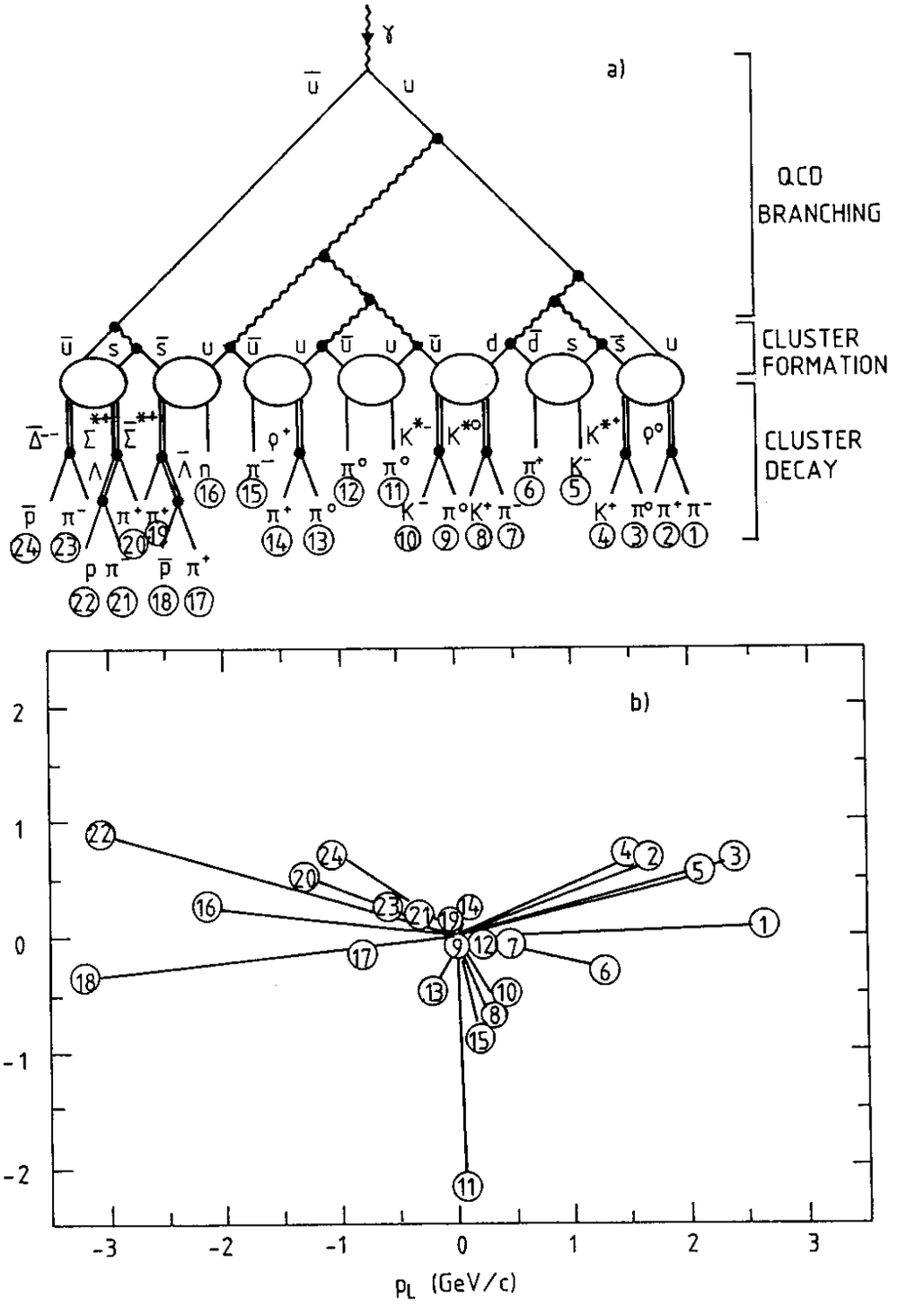
a)
QCD
BRANCHING
CLUSTER
FORMATION
CLUSTER
DECAY
b)
p_{IN} (GeV/c)
p_L (GeV/c)

Fig. 6

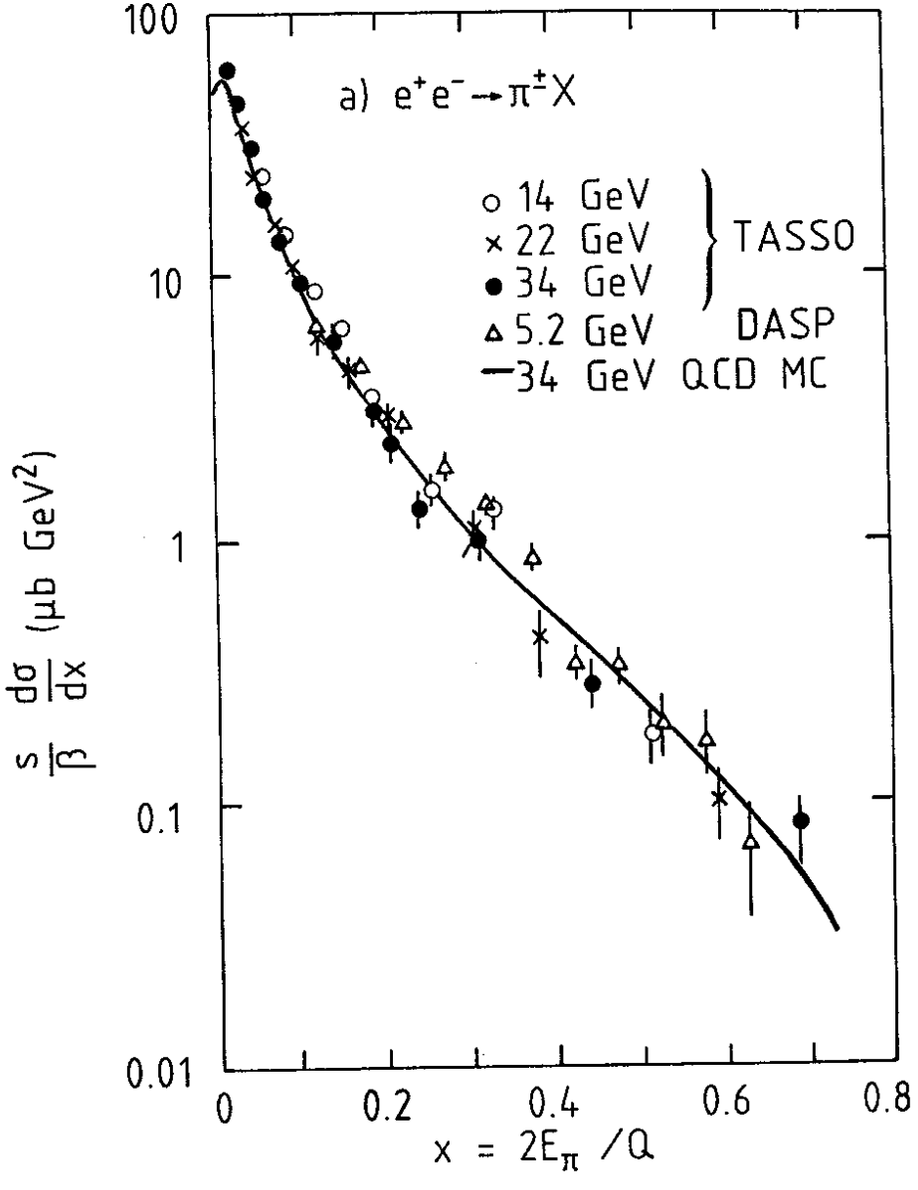
a) $e^+e^- \to \pi^\pm X$
○ 14 GeV
× 22 GeV
● 34 GeV
} TASSO
△ 5.2 GeV DASP
— 34 GeV QCD MC
100
10
1
0.1
0.01
0
0.2
0.4
0.6
0.8
$x = 2E_\pi / Q$
$\frac{s}{\beta} \frac{d\sigma}{dx}$ (μb GeV²)

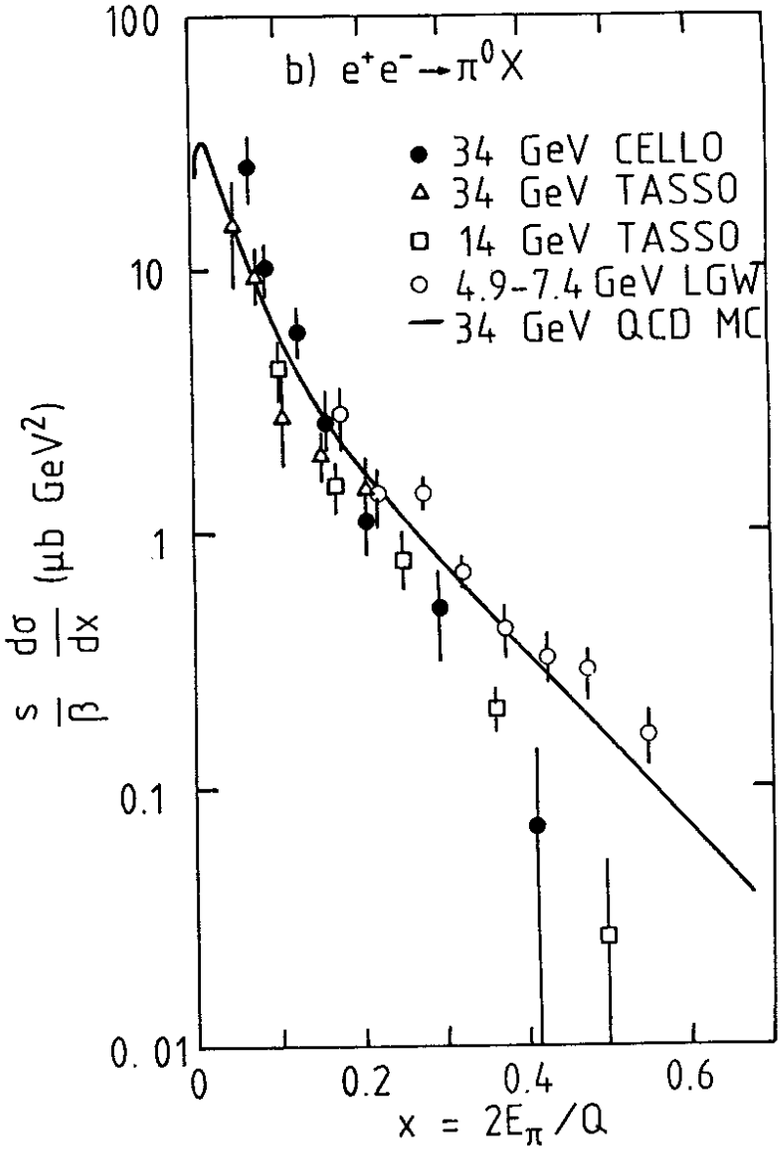
b) $e^+e^- \to \pi^0 X$
● 34 GeV CELLO
△ 34 GeV TASSO
□ 14 GeV TASSO
○ 4.9-7.4 GeV LGW
— 34 GeV QCD MC
100
10
1
0.1
0.01
0
0.2
0.4
0.6
$x = 2E_\pi / Q$
$\frac{s}{\beta} \frac{d\sigma}{dx}$ (μb GeV²)

Fig. 7

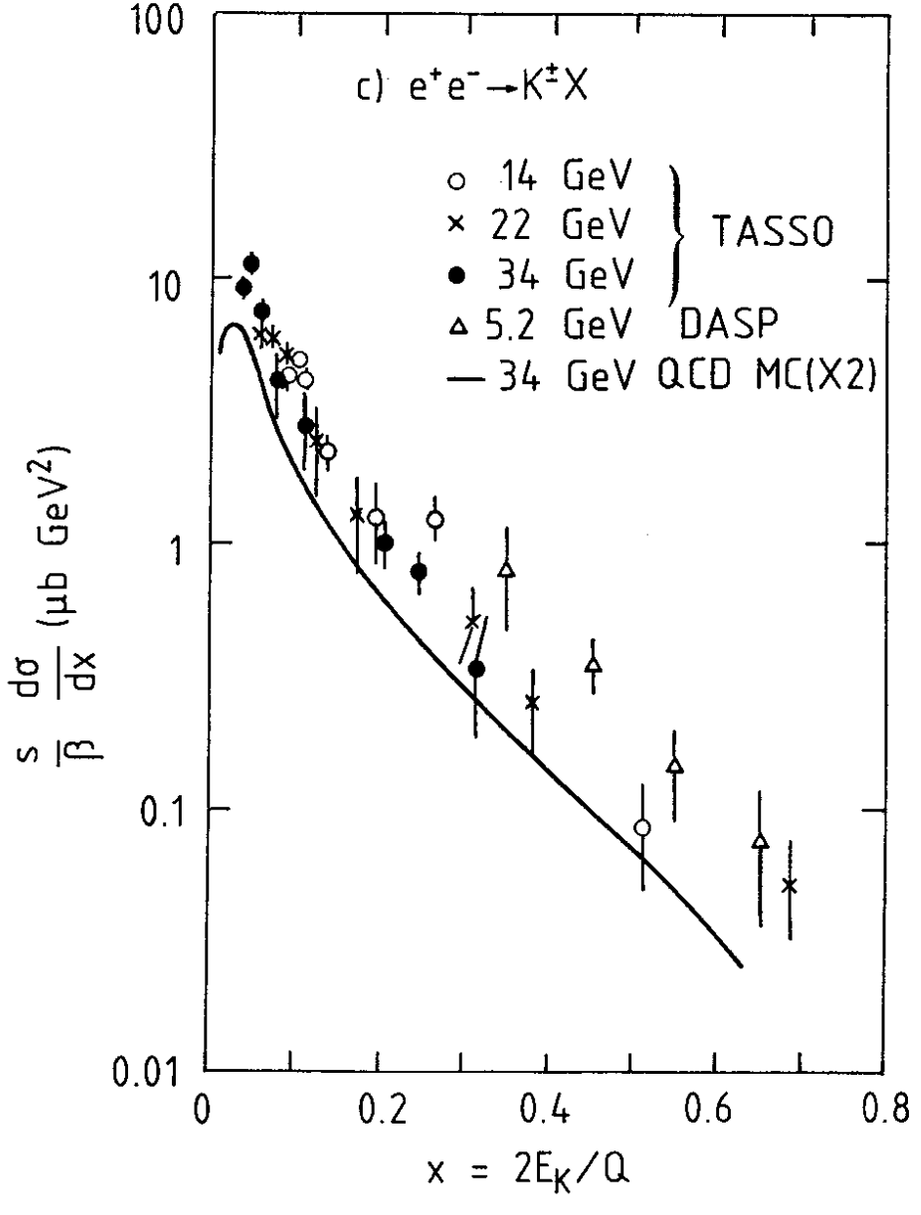
c) $e^+e^- \to K^\pm X$
14 GeV
22 GeV
34 GeV
TASSO
5.2 GeV DASP
34 GeV QCD MC(X2)
$\frac{s}{\beta}\frac{d\sigma}{dx}$ (μb GeV^2)
$x = 2E_K/Q$
100
10
1
0.1
0.01
0
0.2
0.4
0.6
0.8

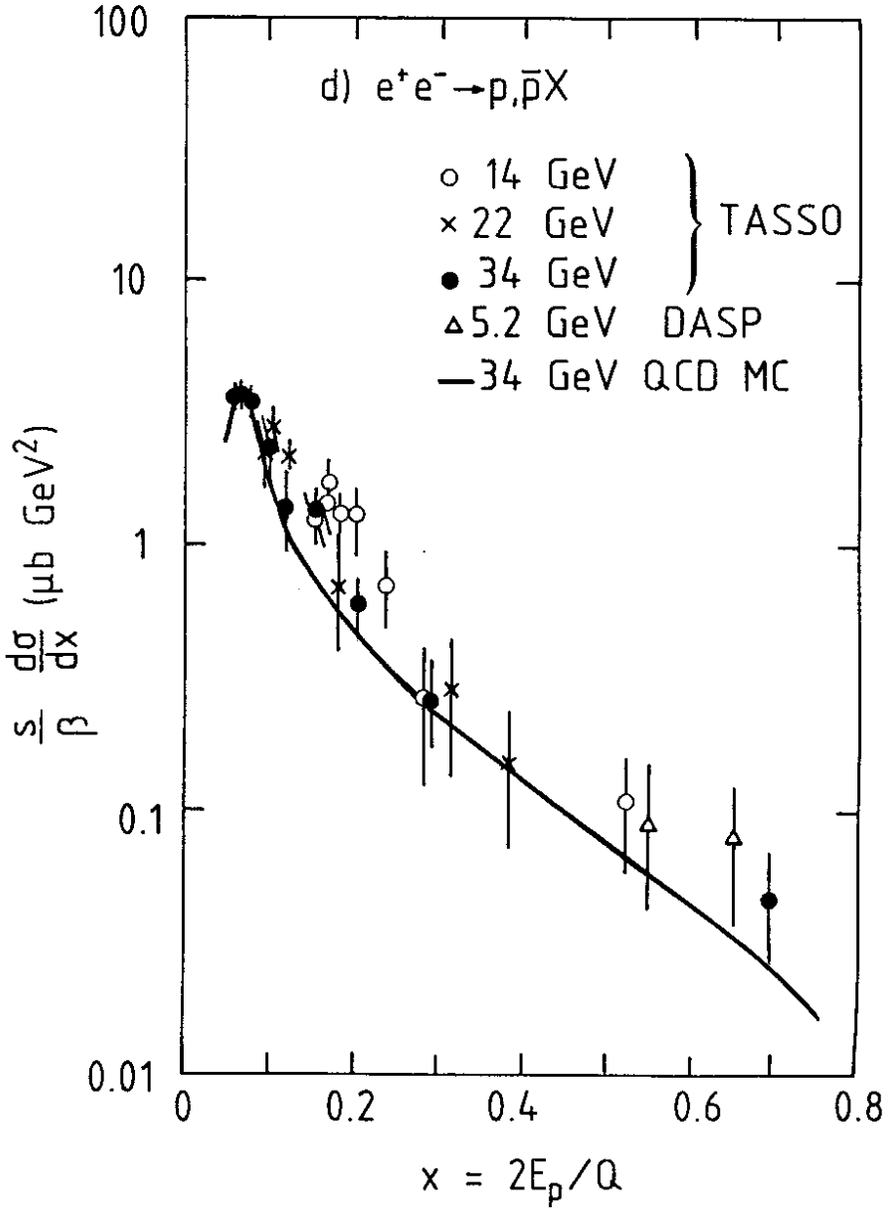
d) $e^+e^- \to p,\bar{p}X$
14 GeV
22 GeV
34 GeV
TASSO
5.2 GeV DASP
34 GeV QCD MC
$\frac{s}{\beta}\frac{d\sigma}{dx}$ (μb GeV^2)
$x = 2E_p/Q$
100
10
1
0.1
0.01
0
0.2
0.4
0.6
0.8

Fig. 7

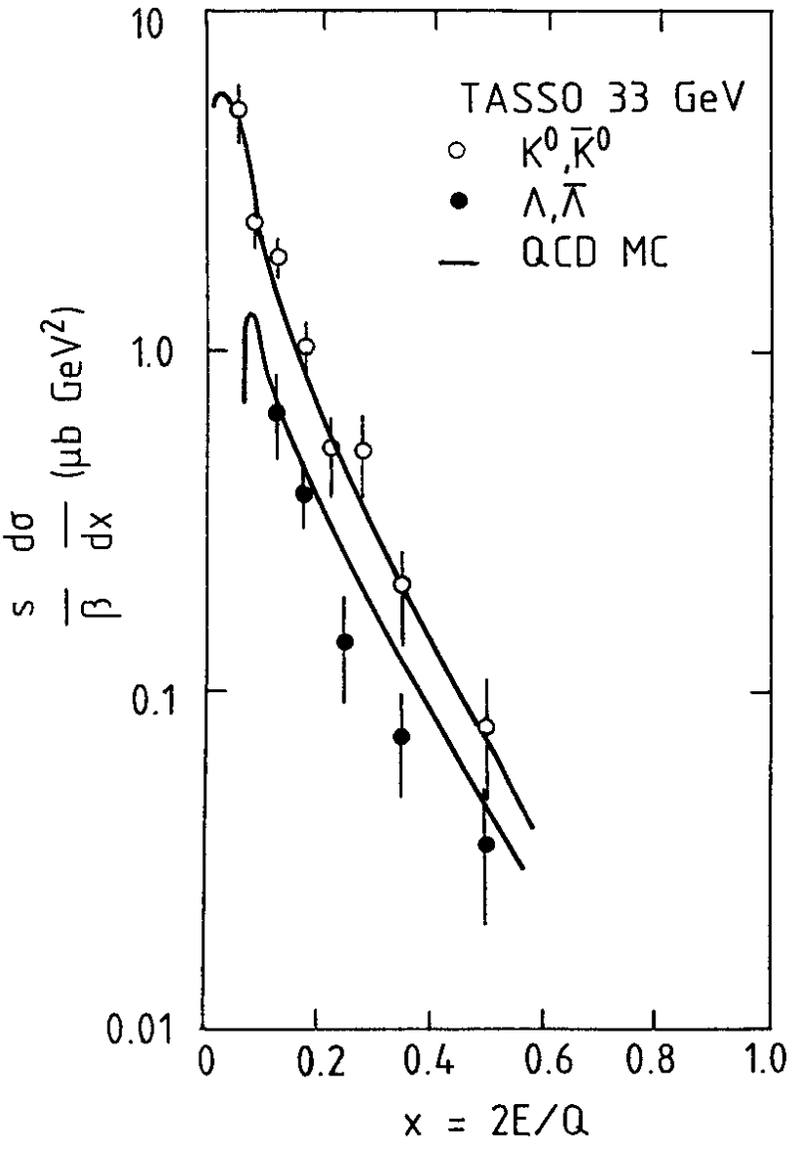
TASSO 33 GeV
$K^0, \bar{K}^0$
$\Lambda, \bar{\Lambda}$
QCD MC
$\frac{s}{\beta} \frac{d\sigma}{dx}$ (μb GeV^2)
10
1.0
0.1
0.01
0
0.2
0.4
0.6
0.8
1.0
x = 2E/Q

Fig. 8

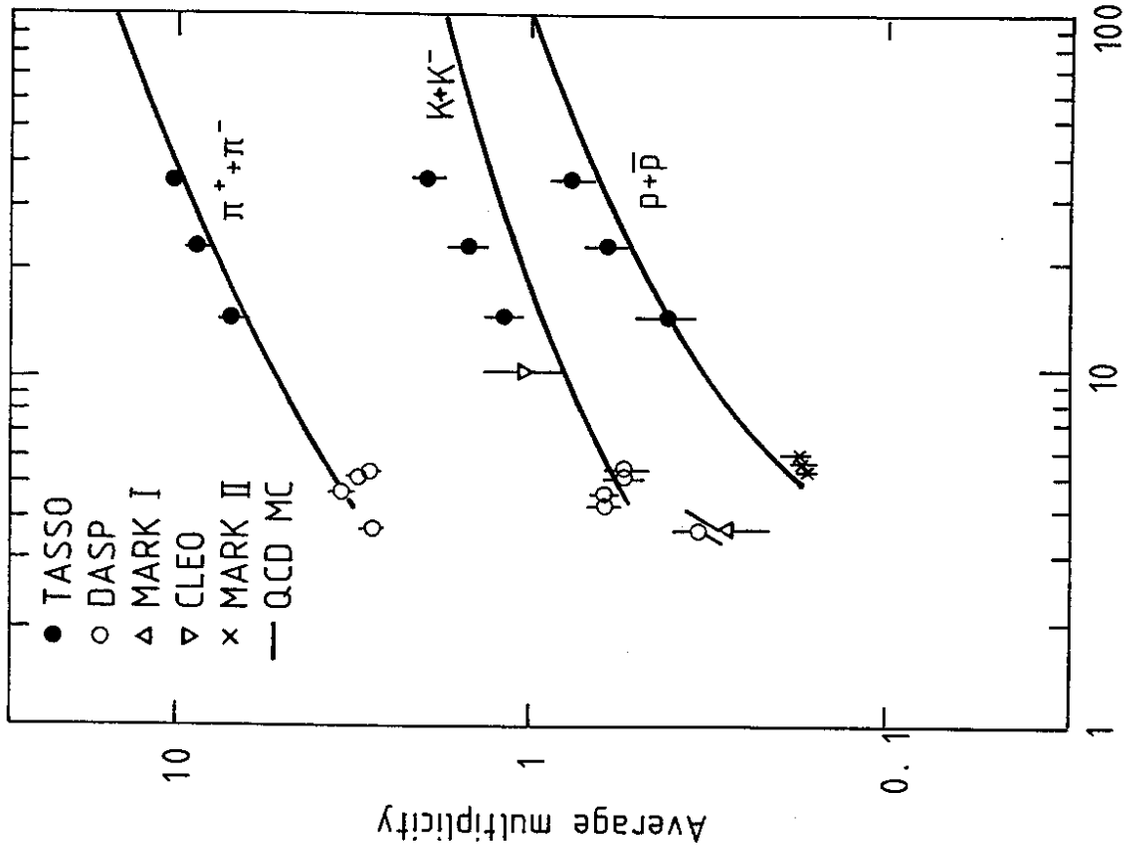
Average multiplicity
Q (GeV)
TASSO
DASP
MARK I
CLEO
MARK II
QCD MC
$\pi^+\pi^-$
K^+K^-
$p\bar{p}$

Fig. 9

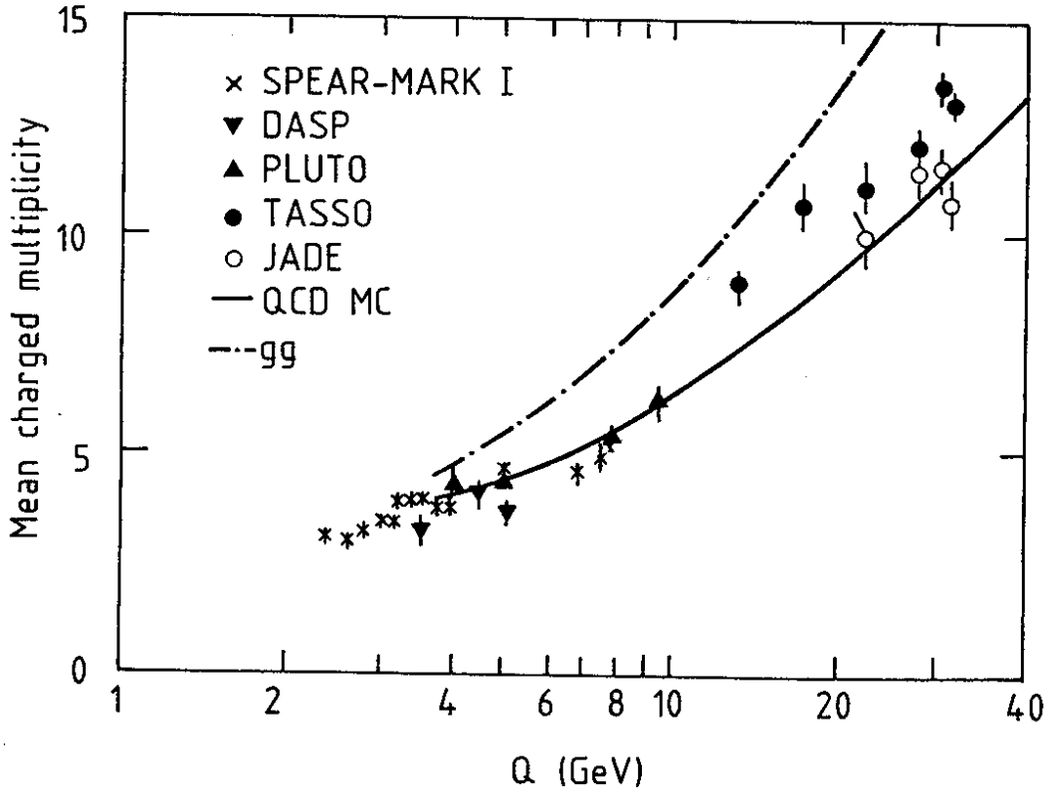
Mean charged multiplicity
Q (GeV)
SPEAR-MARK I
DASP
PLUTO
TASSO
JADE
QCD MC
gg

Fig. 10

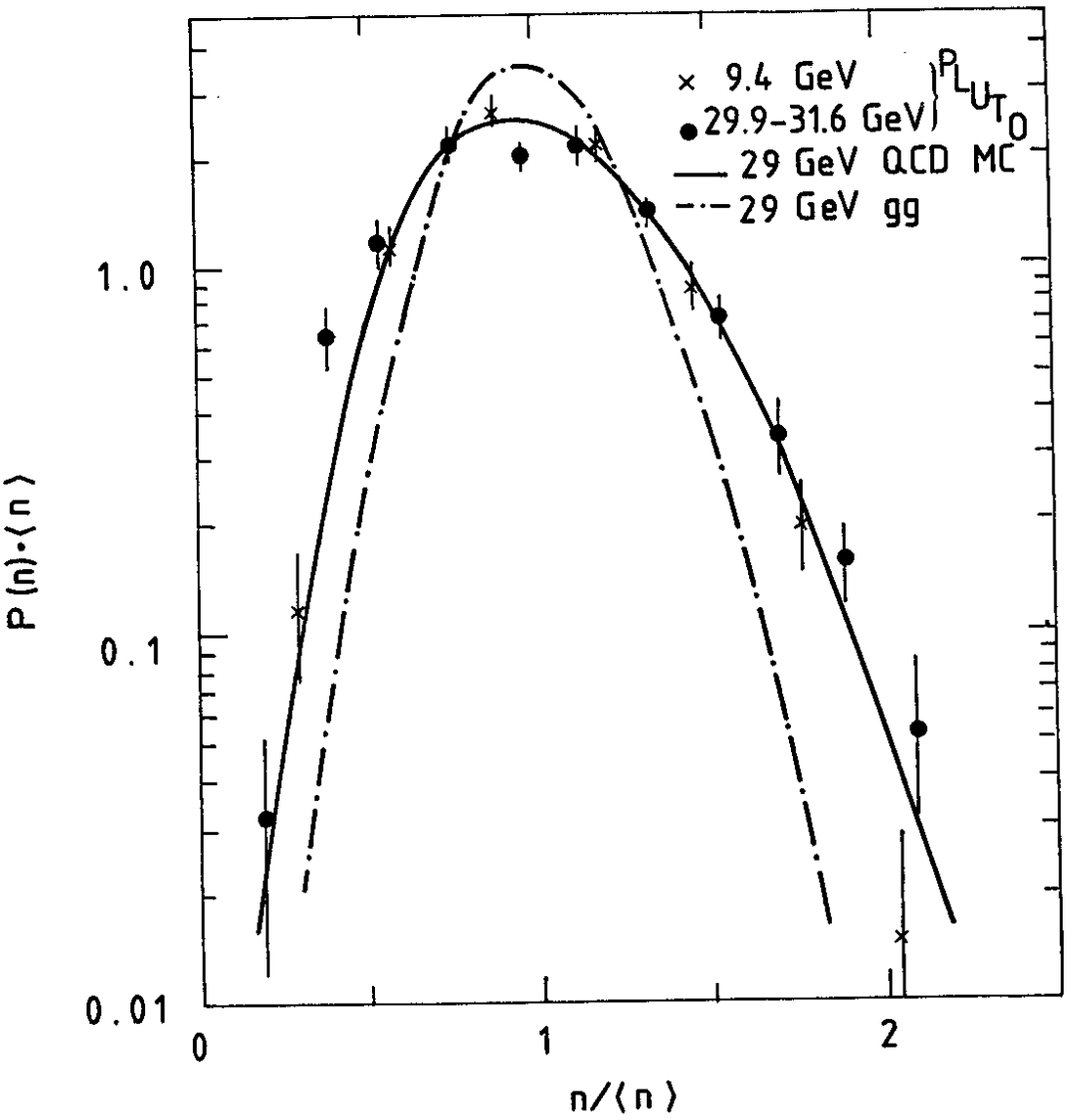
× 9.4 GeV
● 29.9-31.6 GeV
PLUTO
29 GeV QCD MC
29 GeV gg
1.0
0.1
0.01
P(n)·⟨n⟩
0
1
2
n/⟨n⟩

Fig. 11

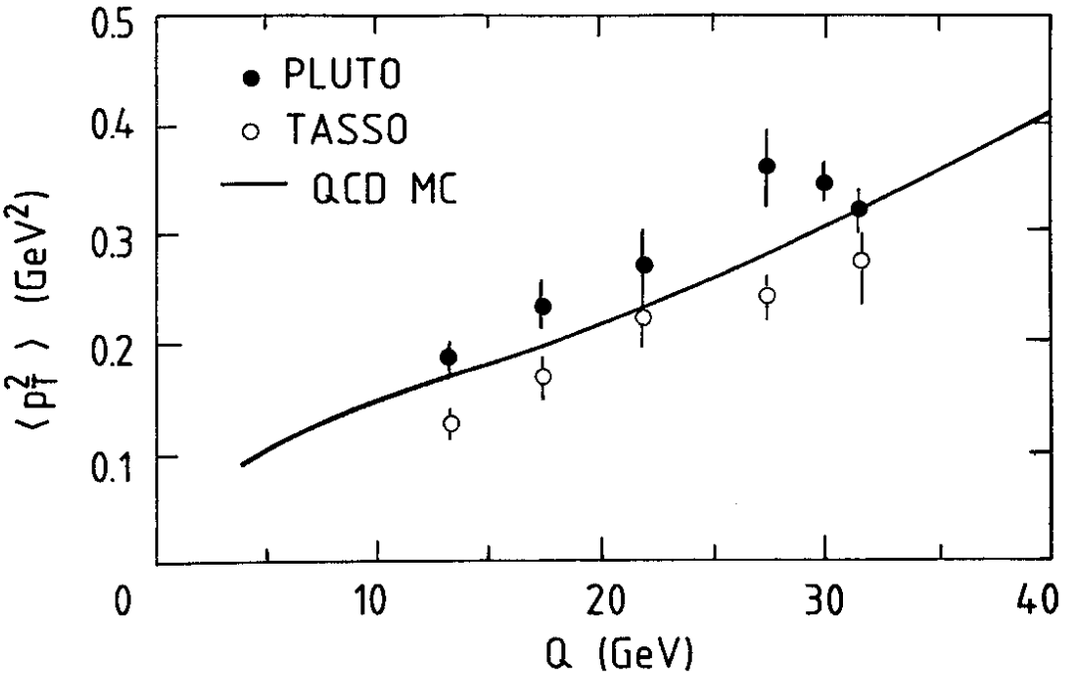
0.5
0.4
0.3
0.2
0.1
0
10
20
30
40
PLUTO
TASSO
QCD MC
$\langle p_T^2 \rangle$ (GeV^2)
Q (GeV)

Fig. 12

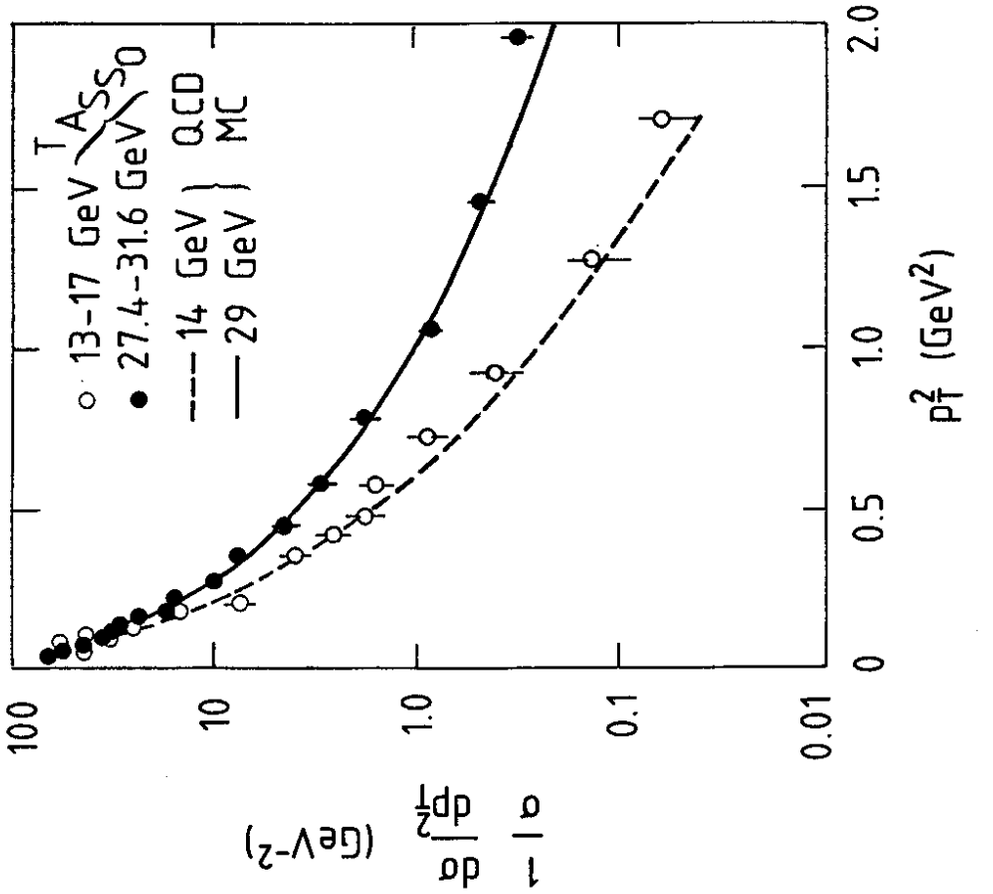
100
10
1.0
0.1
0.01
0
0.5
1.0
1.5
2.0
13-17 GeV
27.4-31.6 GeV
$\sqrt{s}$
14 GeV
29 GeV
QCD
MC
$\frac{1}{\sigma}\frac{d\sigma}{dp_T^2}$ (GeV^{-2})
p_T^2 (GeV^2)

Fig. 13

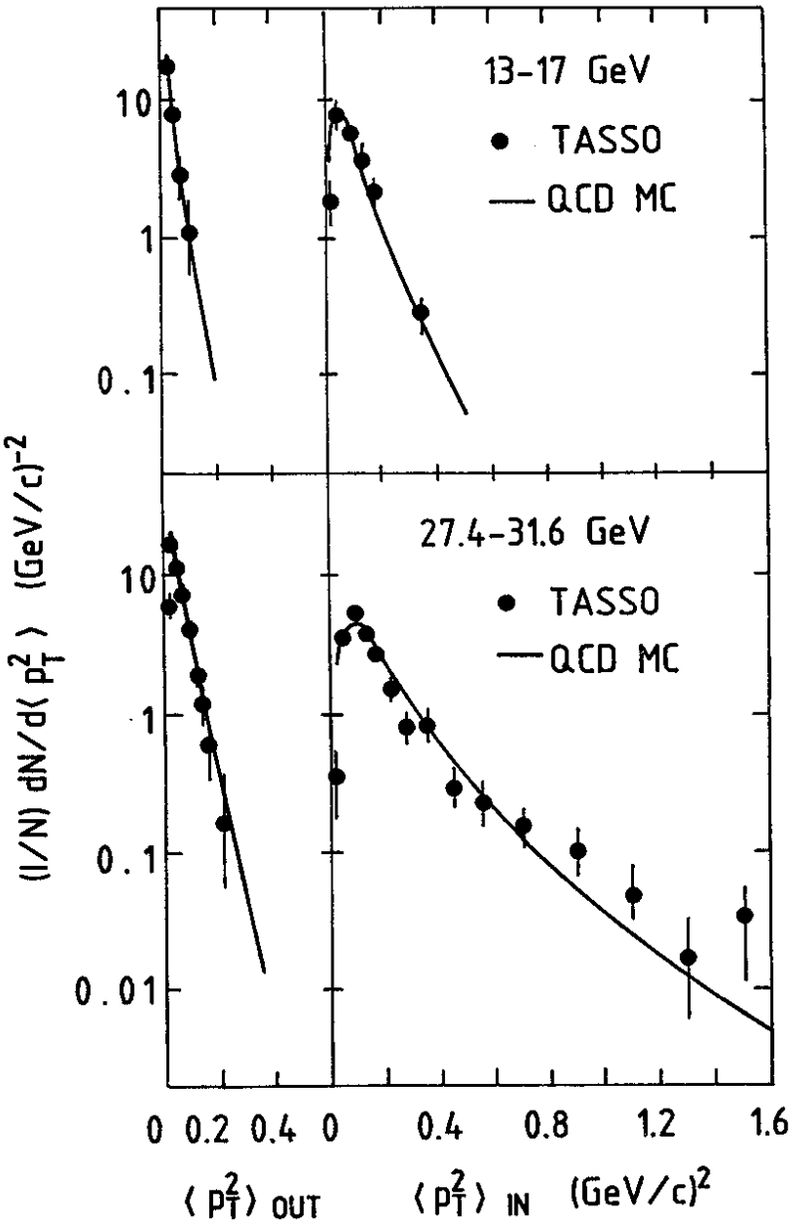
13-17 GeV
TASSO
QCD MC
27.4-31.6 GeV
TASSO
QCD MC
10
1
0.1
0.01
(1/N) dN/d⟨p_T^2⟩ (GeV/c)^-2
0 0.2 0.4
0 0.4 0.8 1.2 1.6
⟨p_T^2⟩ OUT
⟨p_T^2⟩ IN (GeV/c)^2

Fig. 14

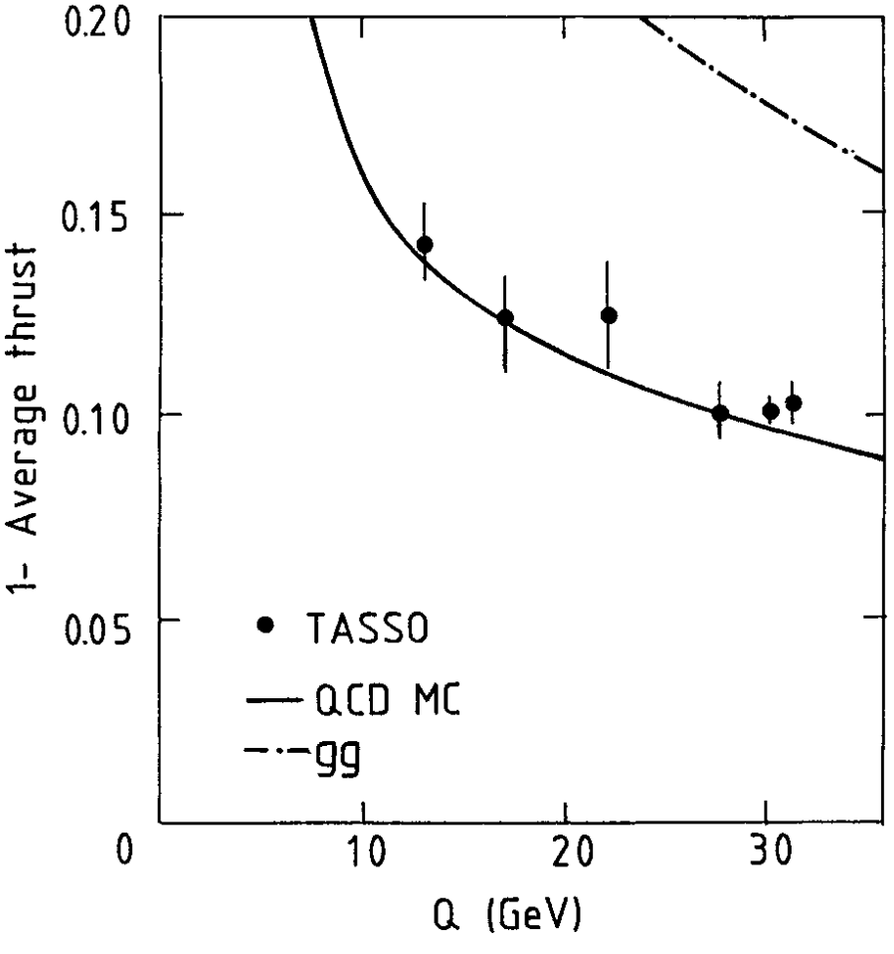
0.20
0.15
0.10
0.05
0
1- Average thrust
TASSO
QCD MC
gg
10
20
30
Q (GeV)

Fig. 15

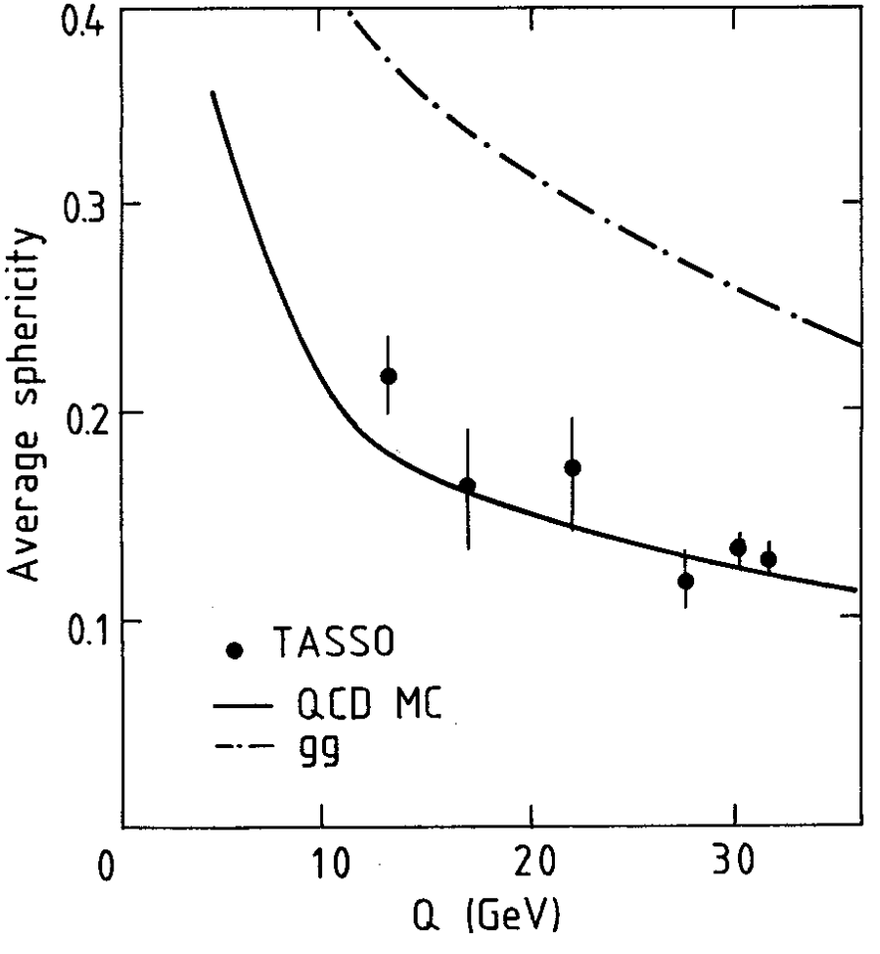
0.4
0.3
0.2
0.1
0
Average sphericity
TASSO
QCD MC
gg
10
20
30
Q (GeV)

Fig. 16

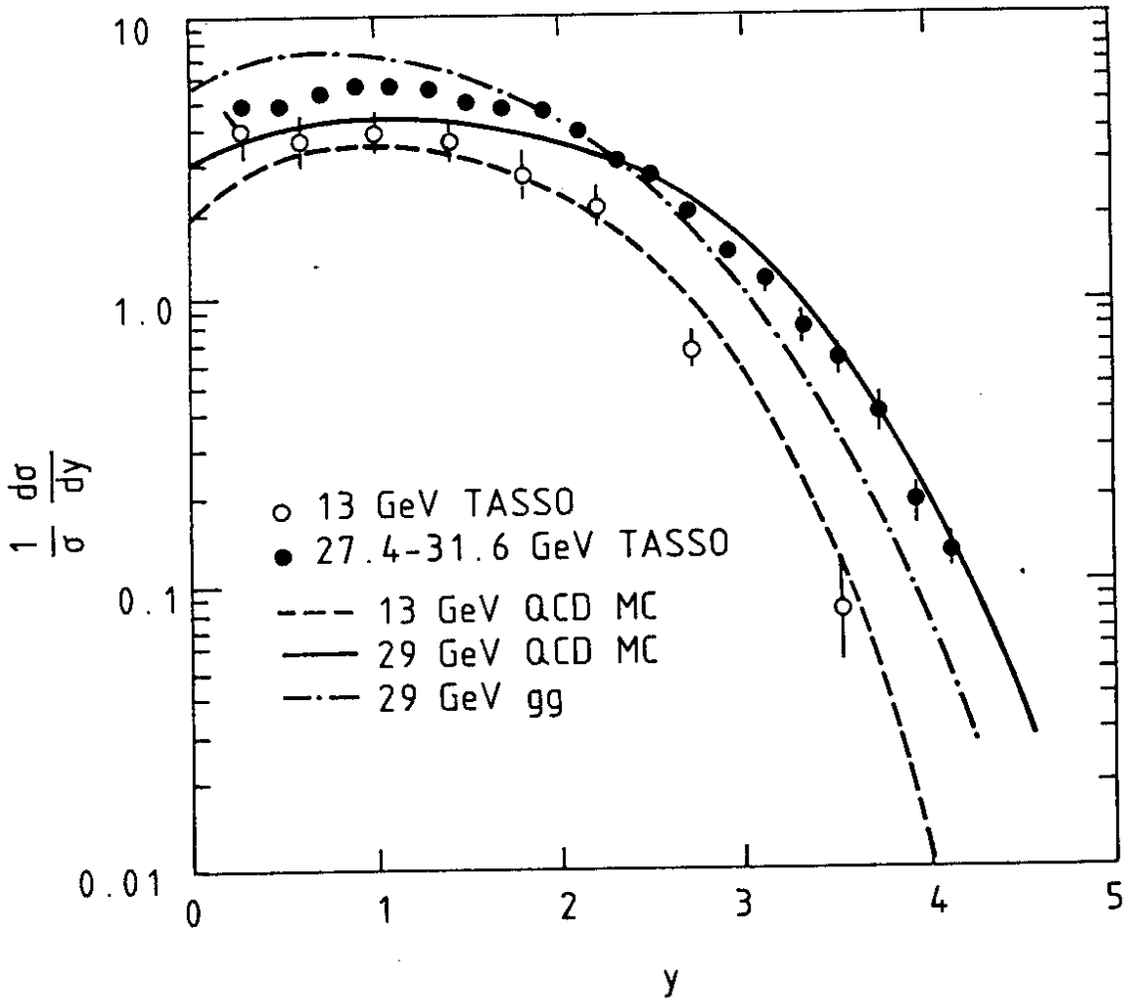
10
1.0
0.1
0.01
0
1
2
3
4
5
y
1/σ dσ/dy
13 GeV TASSO
27.4-31.6 GeV TASSO
13 GeV QCD MC
29 GeV QCD MC
29 GeV gg

Fig. 17

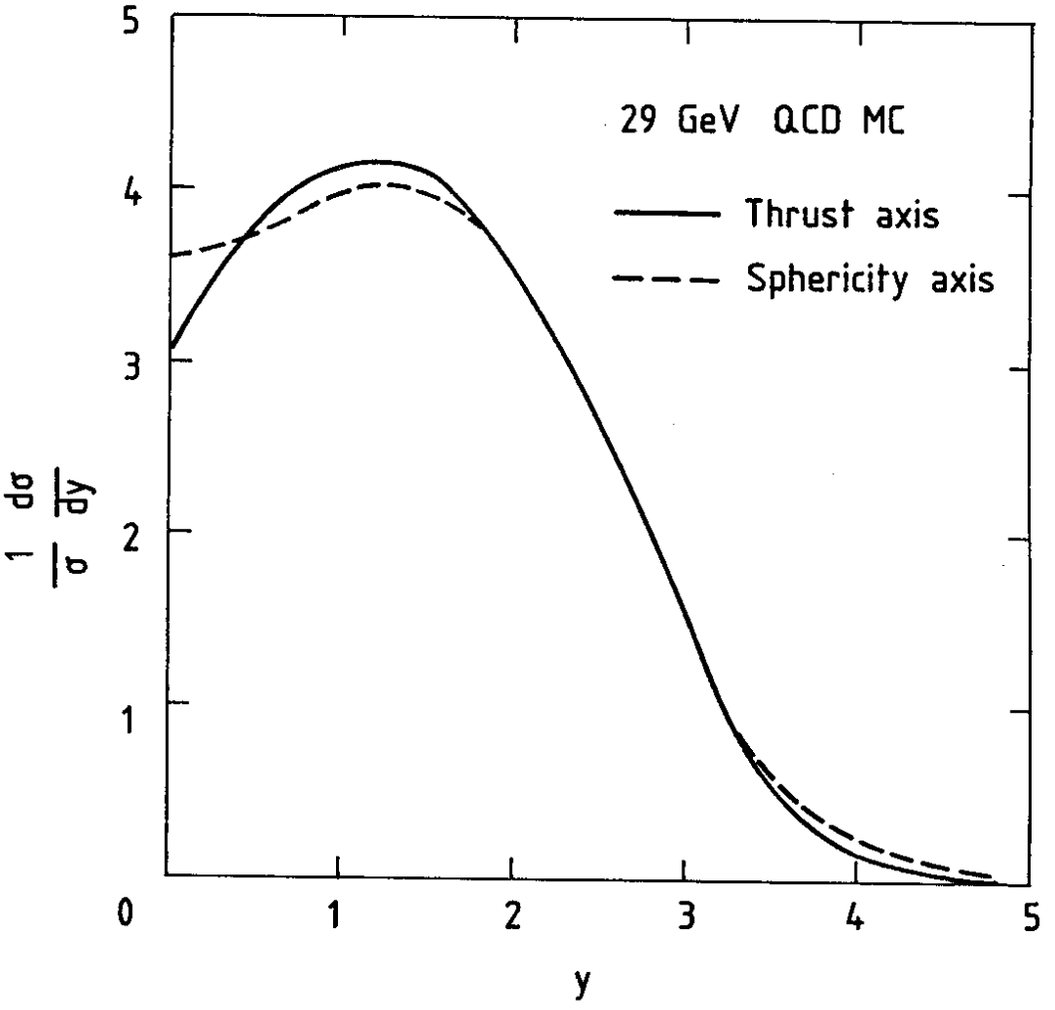

Fig. 18

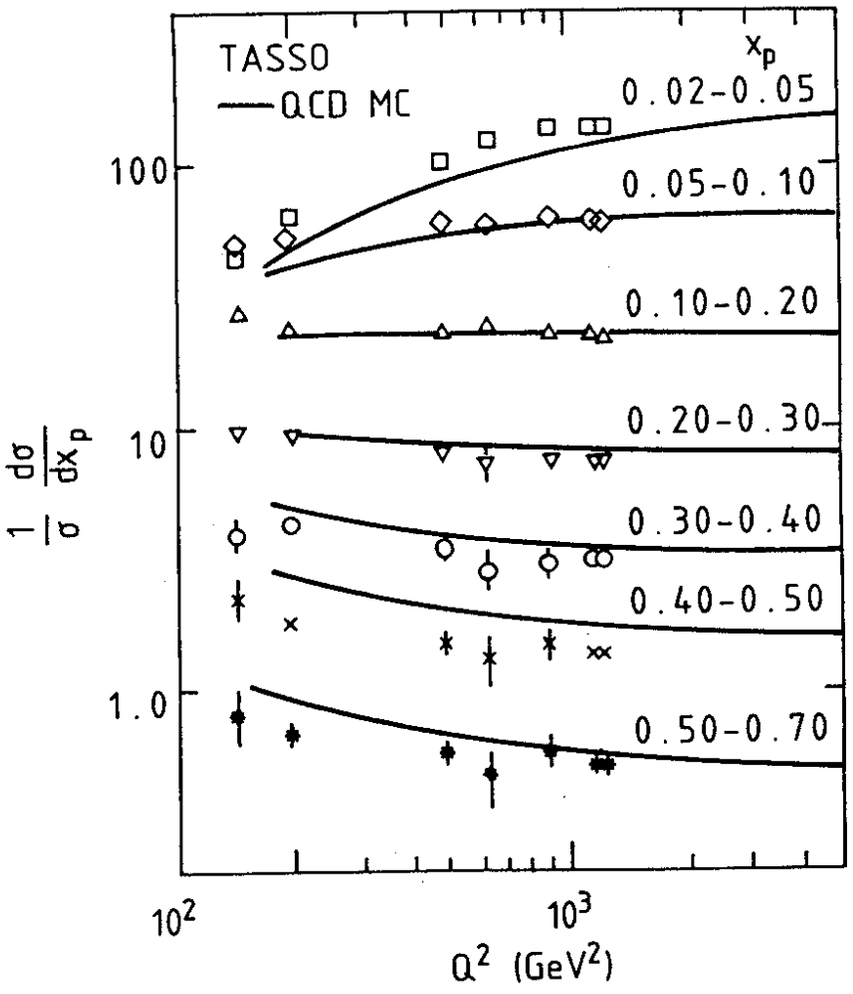
TASSO
QCD MC
x_p
0.02-0.05
0.05-0.10
0.10-0.20
0.20-0.30
0.30-0.40
0.40-0.50
0.50-0.70
100
10
1.0
$\frac{1}{\sigma}\frac{d\sigma}{dx_p}$
10^2
10^3
Q^2 (GeV^2)

Fig. 19

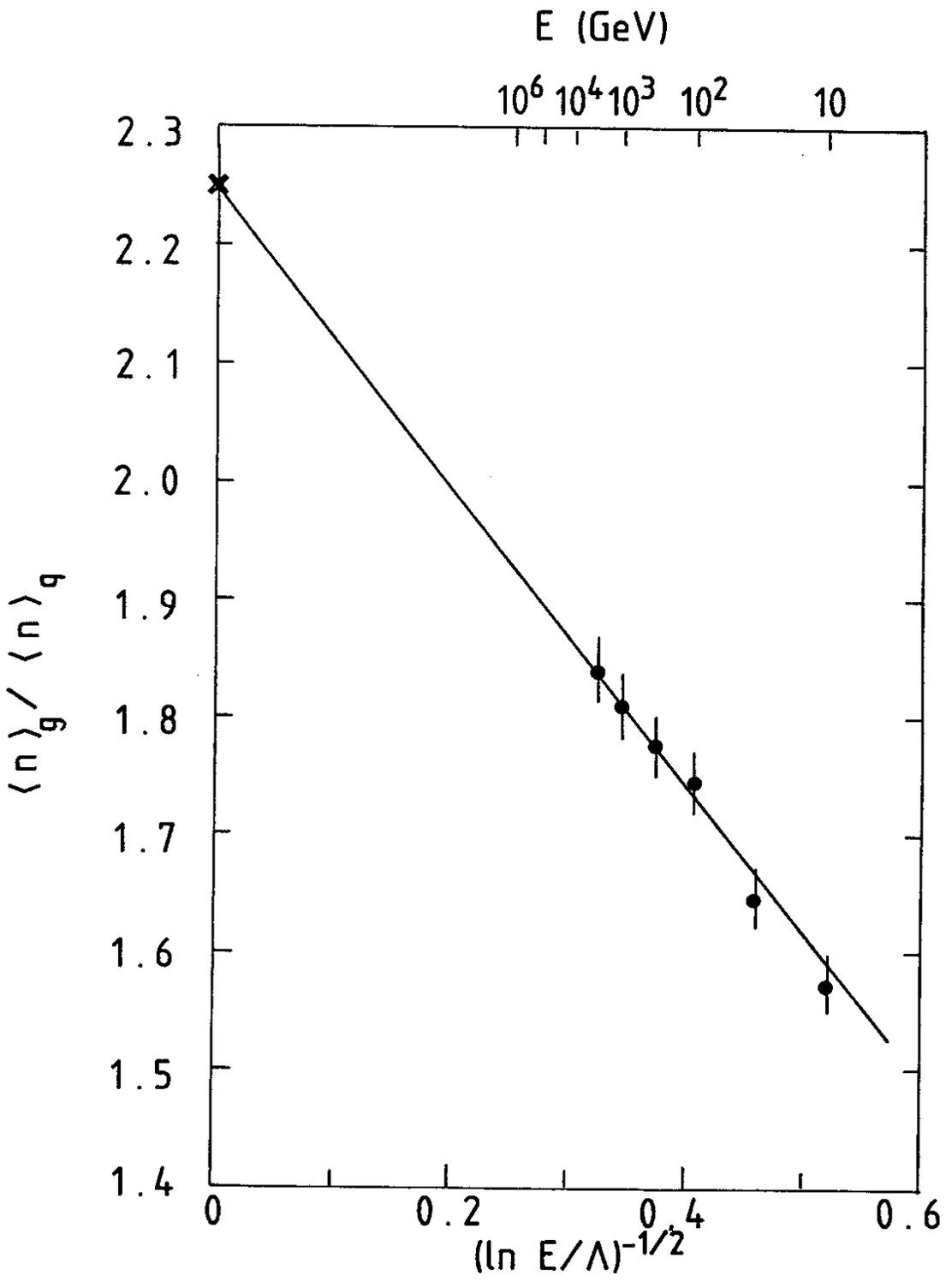
E (GeV)
10^6 10^4 10^3 10^2 10
2.3
2.2
2.1
2.0
1.9
1.8
1.7
1.6
1.5
1.4
$\langle n \rangle_g / \langle n \rangle_q$
0
0.2
0.4
0.6
$(\ln E/\Lambda)^{-1/2}$

Fig. 20

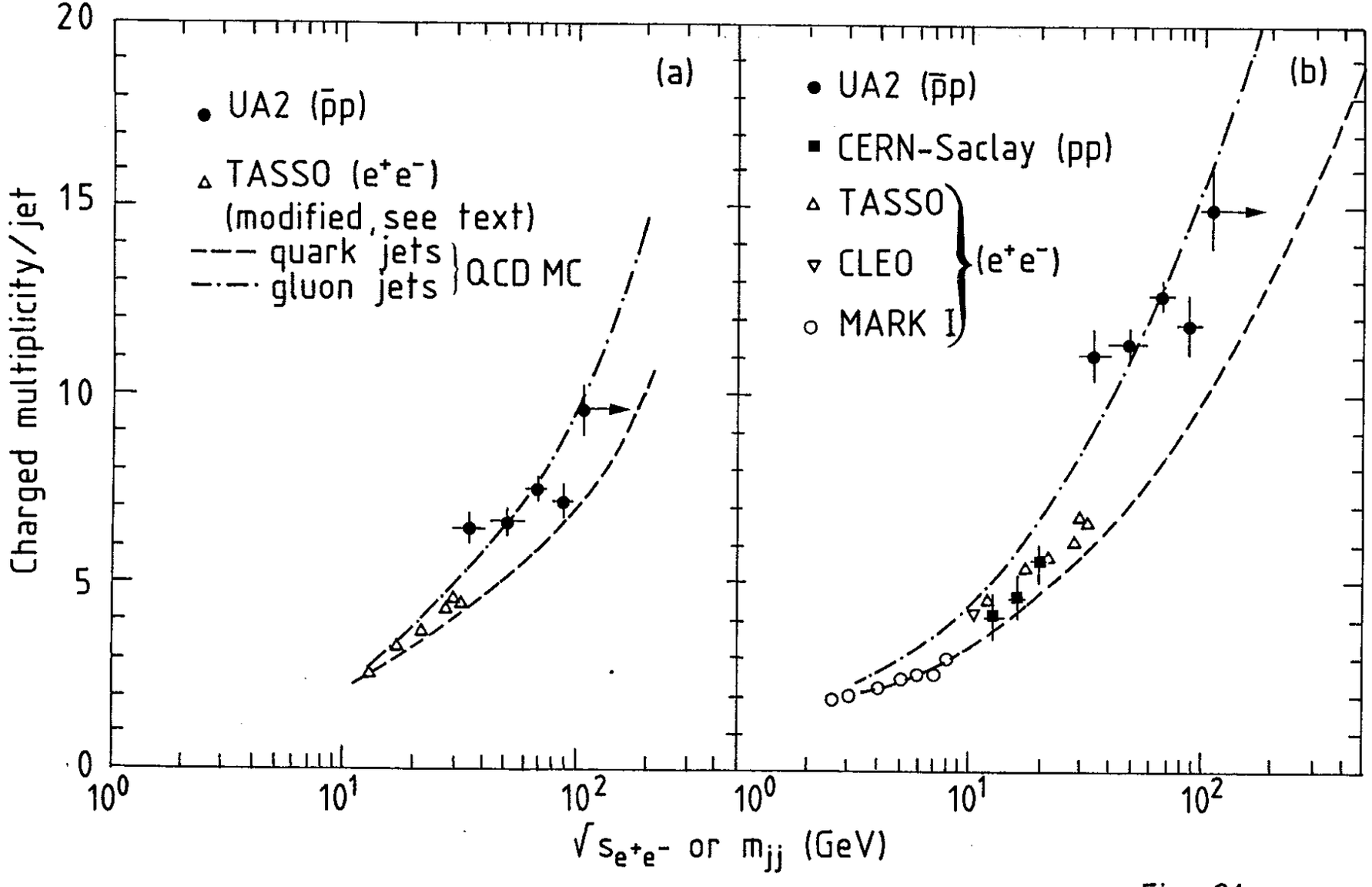
20
15
10
5
0
Charged multiplicity/jet
(a)
UA2 ($\bar{p}p$)
TASSO (e^+e^-)
(modified, see text)
quark jets
gluon jets
QCD MC
(b)
UA2 ($\bar{p}p$)
CERN-Saclay (pp)
TASSO
CLEO
MARK I
(e^+e^-)
10^0
10^1
10^2
$\sqrt{s}_{e^+e^-}$ or m_{jj} (GeV)

Fig. 21

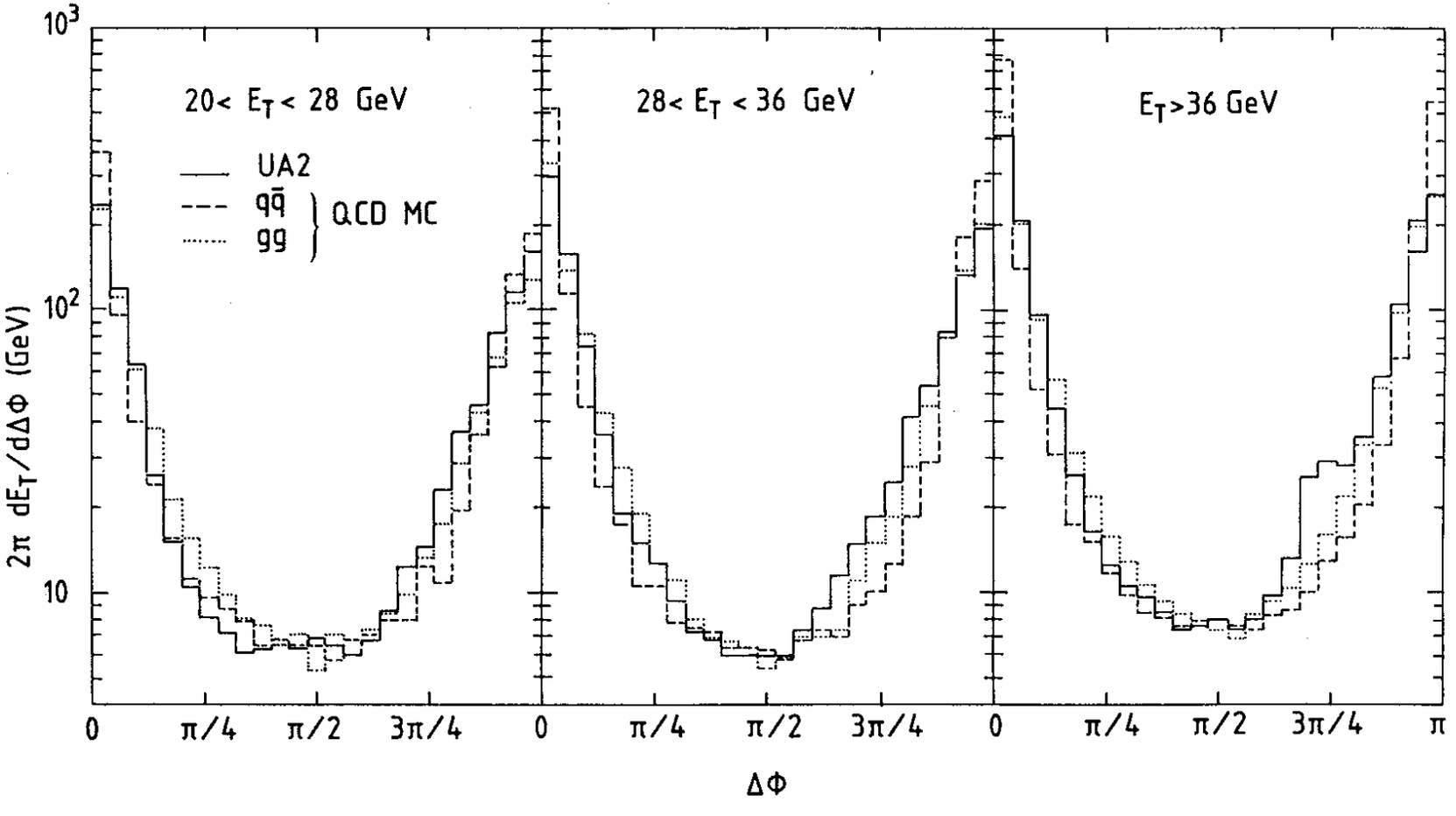
10^3
10^2
10
$2\pi\ dE_T/d\Delta\Phi$ (GeV)
$20< E_T < 28$ GeV
$28< E_T < 36$ GeV
$E_T > 36$ GeV
UA2
$q\bar{q}$
gg
QCD MC
0
$\pi/4$
$\pi/2$
$3\pi/4$
π
$\Delta\Phi$

Fig. 22

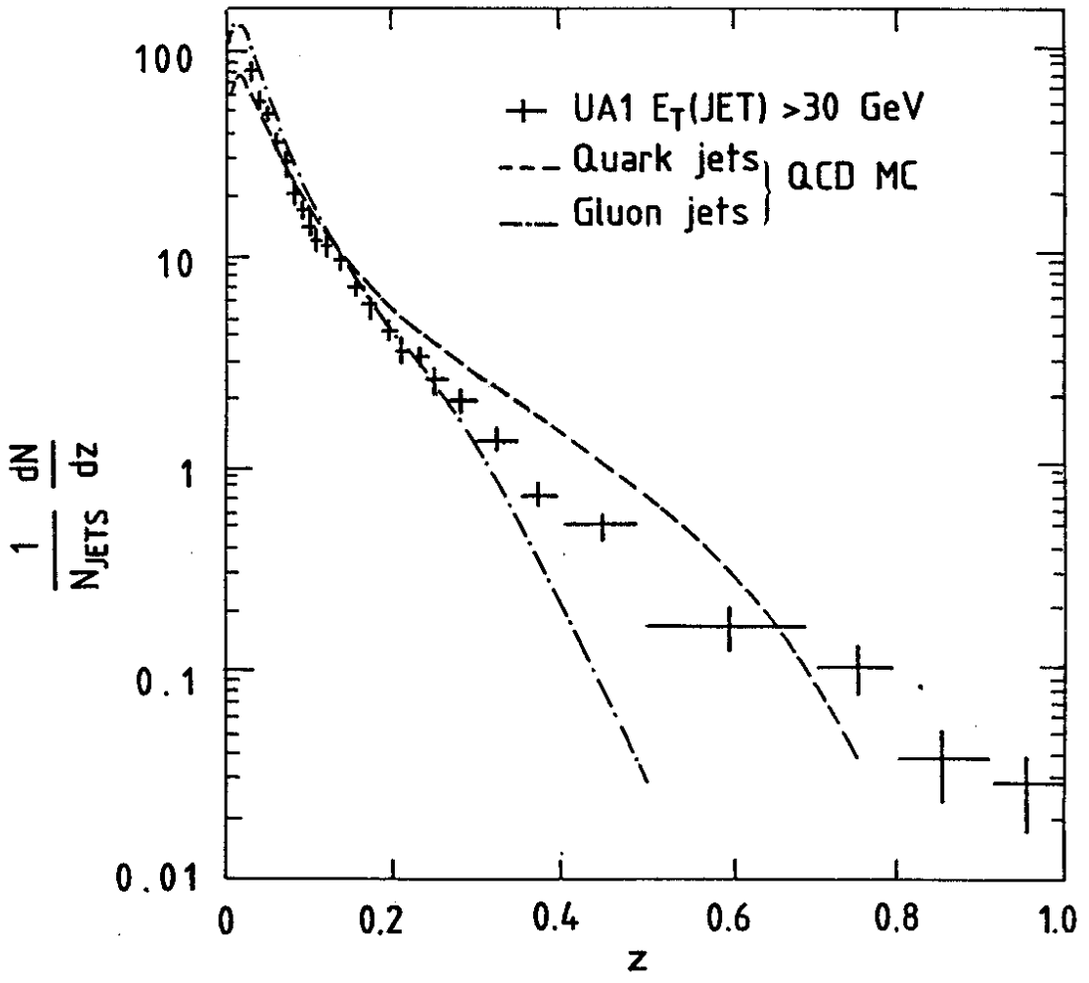
100
10
1
0.1
0.01
0
0.2
0.4
0.6
0.8
1.0
z
$\frac{1}{N_{JETS}} \frac{dN}{dz}$
UA1 E_T(JET) >30 GeV
Quark jets
Gluon jets
QCD MC

Fig. 23

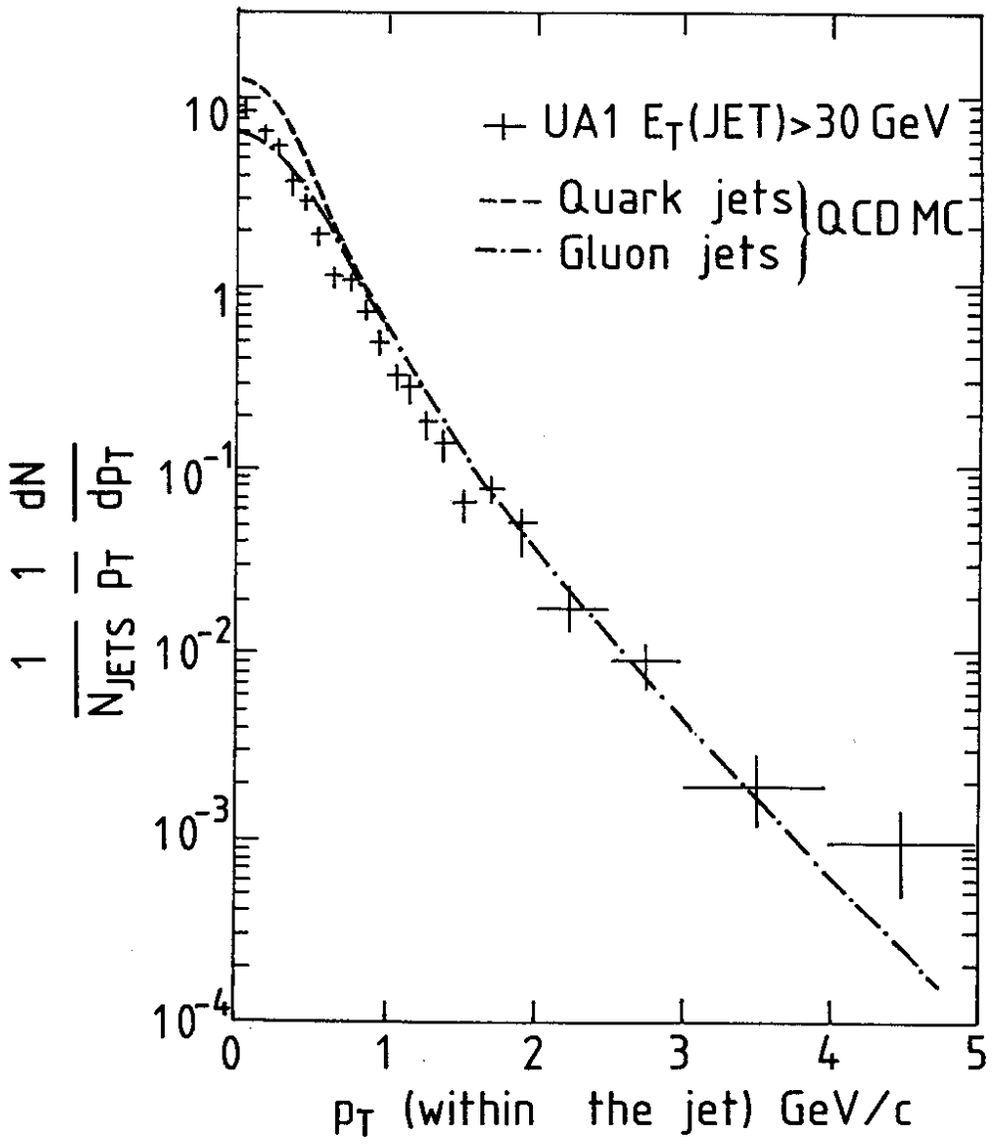
+ UA1 E_T(JET)>30 GeV
--- Quark jets
-·- Gluon jets
QCD MC
$\frac{1}{N_{JETS}} \frac{1}{p_T} \frac{dN}{dp_T}$
p_T (within the jet) GeV/c
10
1
10^{-1}
10^{-2}
10^{-3}
10^{-4}
0
1
2
3
4
5

Fig. 24

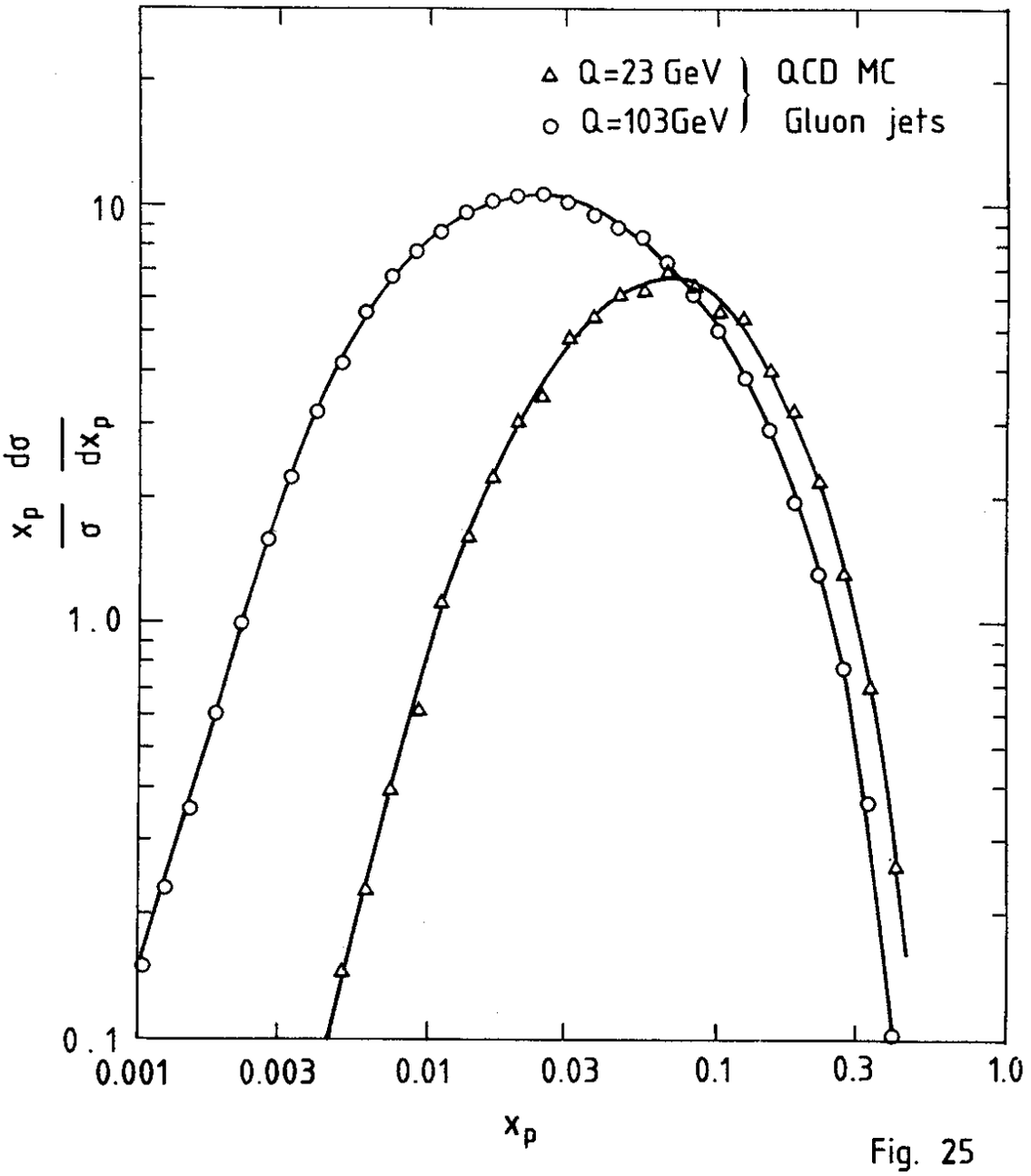
Δ Q=23 GeV
○ Q=103GeV
QCD MC
Gluon jets
10
1.0
0.1
0.001
0.003
0.01
0.03
0.1
0.3
1.0
x_p
$\frac{x_p}{\sigma}\frac{d\sigma}{dx_p}$

Fig. 25

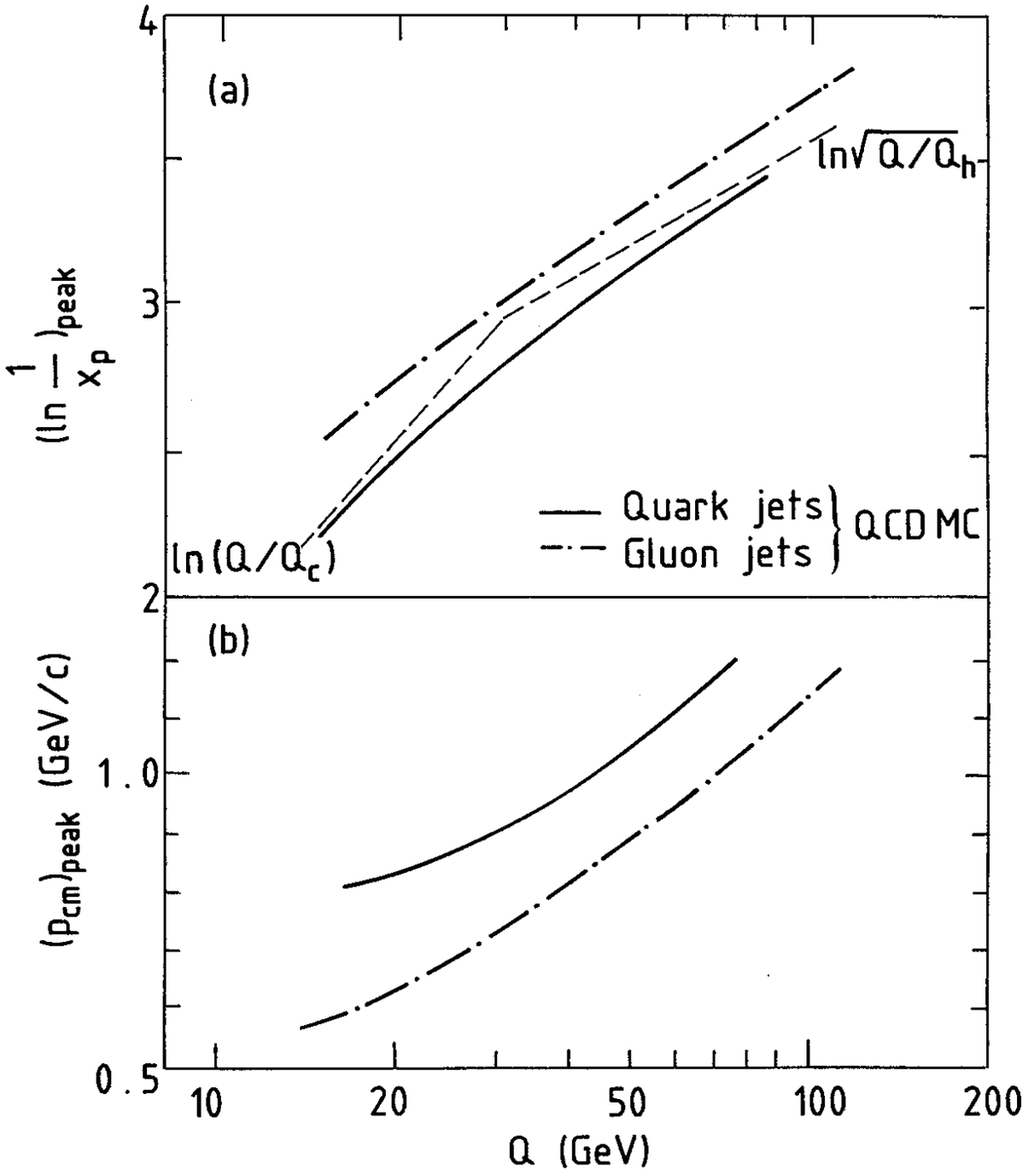
(a)
(b)
$\ln\sqrt{Q/Q_h}$
$\ln(Q/Q_c)$
Quark jets
Gluon jets
QCD MC
$(\ln\frac{1}{x_p})_{peak}$
$(p_{cm})_{peak}$ (GeV/c)
Q (GeV)
4
3
2
1.0
0.5
10
20
50
100
200

Fig. 26

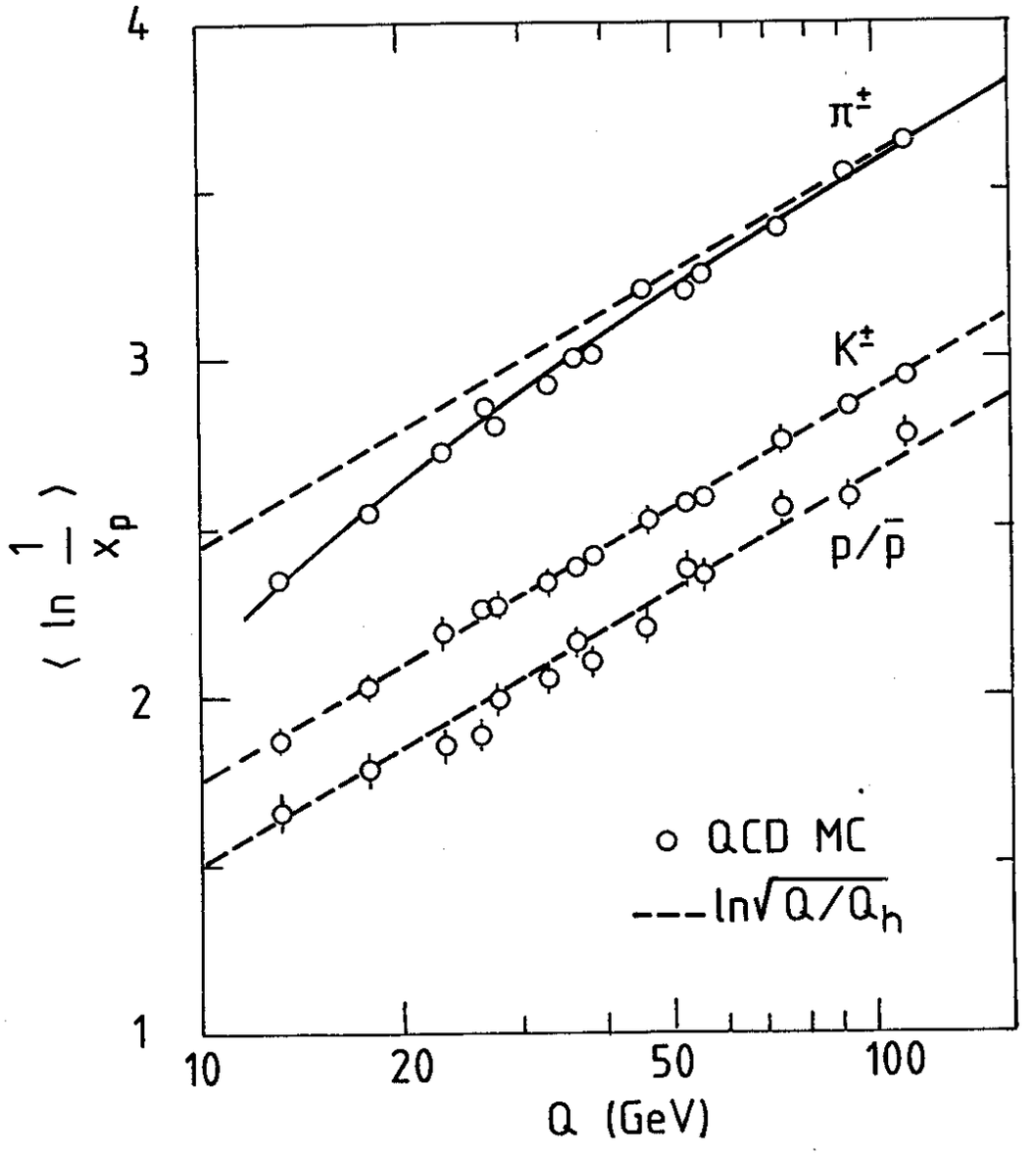

Fig. 27